Chapter 6

Validation – Derivation of Cirrus Cloud Properties from MIPAS data

One of the crucial characteristics of SARTre is the ability to model limb emission observations that are influenced by scattered radiation. Scattering in the infrared and microwave spectral region is generally caused by high altitude ice clouds. Taking scattering into account, when modeling and analyzing thermal emission spectra, may help to improve the retrieval of temperature and trace gas profiles on the one hand. On the other hand, it allows to derive properties of ice clouds, with limb spectra in particular enabling to observe very thin (subvisible) clouds, which are invisible to nadir looking instruments.

In this chapter the effect of thin and subvisible cirrus clouds on mid-infrared limb spectra is studied. To validate the SARTre model, simulated spectra are set in contrast to cirrus features observed in MIPAS data. From comparison of modeled and measured spectra, cloud properties are estimated.

6.1 The MIPAS Data Set

MIPAS, the Michelson Interferometer for Passive Atmospheric Sounding (Fischer and Oelhaf, 1996) is a Fourier transform spectrometer onboard the European ENVISAT mission, measuring limb emission spectra over five channels covering the mid-infrared region between $685-2410\,\mathrm{cm}^{-1}$ ($4.15-14.6\,\mu\mathrm{m}$). With its high spectral resolution of $0.035\,\mathrm{cm}^{-1}$ (FWHM, unapodized) resulting from a maximum optical path difference of 20 cm, MIPAS is designed for the monitoring of trace gas species. A nominal MIPAS limb sequence consists of 17 limb scans between approximately $6-68$ km with a vertical spacing of 3 km between $3-42$ km and and a spacing between 6 km and 8 km for upper tangent altitudes (from top to down named sweep 0 to 16). At the tangent point, the nominal field of view (FOV) is about 3 km in vertical by 30 km in horizontal direction. Noise Equivalent Spectral Radiance (NESR) of MIPAS is between $0.5\,\mathrm{mW/(m^2\,sr\,cm^{-1})}$ at $685\,\mathrm{cm}^{-1}$ and $0.04\,\mathrm{mW/(m^2\,sr\,cm^{-1})}$ at $2410\,\mathrm{cm}^{-1}$ (Steck, 2000).

For validation of the SARTre model MIPAS data was searched for a limb sequence, where spectra of tangent altitudes in the upper troposphere and/or lower stratosphere show distinct spectral features of thin high altitude clouds:

1. a significant increased broadband continuum signal in the region of atmospheric windows
2. broad absorption line structures, e.g. of H_2O, instead of narrow emission lines in clear-sky spectra.

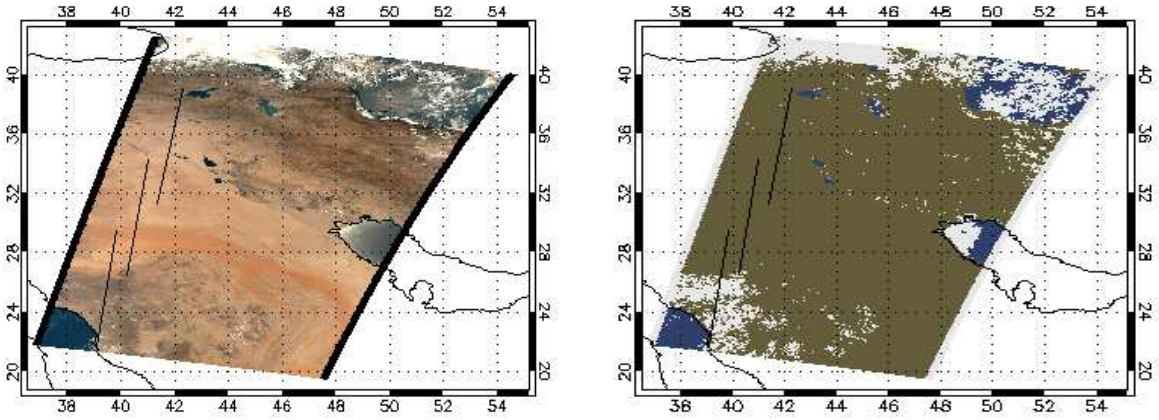

Figure 6.1: *RGB-composite and cloud mask from MERIS data of ENVISAT orbit 7203 (courtesy of Institute for Space Sciences, Free University Berlin), taken approximately 15 min before the MIPAS data. Black lines indicate MIPAS lines of sight below 30 km for subsequent limb sequences (from north to south) T0727, T0728 and T0730 (the latter not examined within this work).*

Cloud indices, as proposed by Spang et al. (2004) and routinely calculated at the Institute of Meteorology and Climate Research Karlruhe (IMK) when processing Level-1B data, allow for fast decision about the occurence of criterion 1. Being defined as ratio of mean intensity in a spectral region dominated by CO_2 and O_3 emission to the intensity in a window region dominated by cloud and aerosol emission and scattering, large cloud indices correspond to clear-sky measurements while low indices indicate cloud or dense aerosol layers in the line of sight (LOS). Therefore, a number of candidate MIPAS limb sequences was chosen with low cloud index at high tropospheric tangent altitudes and higher indices at subsequent lower tangent altitudes, decreasing the probability of a second cloud layer below. Candidate spectra were visually inspected for fulfilling of criterion 2. To assure absence of low water clouds in order to avoid further complex simulation setup, MERIS and MODIS cloud data were used.

Finally, limb sequence 07203_20030717T072843Z (in the following referred to as T0728) of orbit 7203 from July, 17th, 2003 has been chosen. This limb sequence was taken over Arabian peninsula (mean tangent point location at 30.0 °N 41.0 °E) at about 10:30 am local time (see Fig. 6.1). Examination of cirrus cloud effects will focus on sweeps 13 and 14 with tangent altitudes of about 15 km and 12 km. The previous limb sequence 07203_20030717T072722Z (T0727) is used to illustrate clear-sky in contrast to cloud influenced spectra. Spectra of tangent altitudes between 18 km down to 12 km (sweeps 12 – 14) of sequences T0727 and T0728 are shown in Fig. 6.2.

6.2 Observation and Simulation of High Altitude Ice Clouds

6.2.1 Effects of High Clouds to Infrared Spectra

The important role of high altitude clouds, e.g. on the global radiation budget, had already been demonstrated three decades ago (Stephens and Webster, 1981; Platt, 1981). Improvement of knowledge about global cloud properties has been identified as one of the major tasks in climate research around the same time (Schiffer and Rossow, 1983), leading to the establishment of the

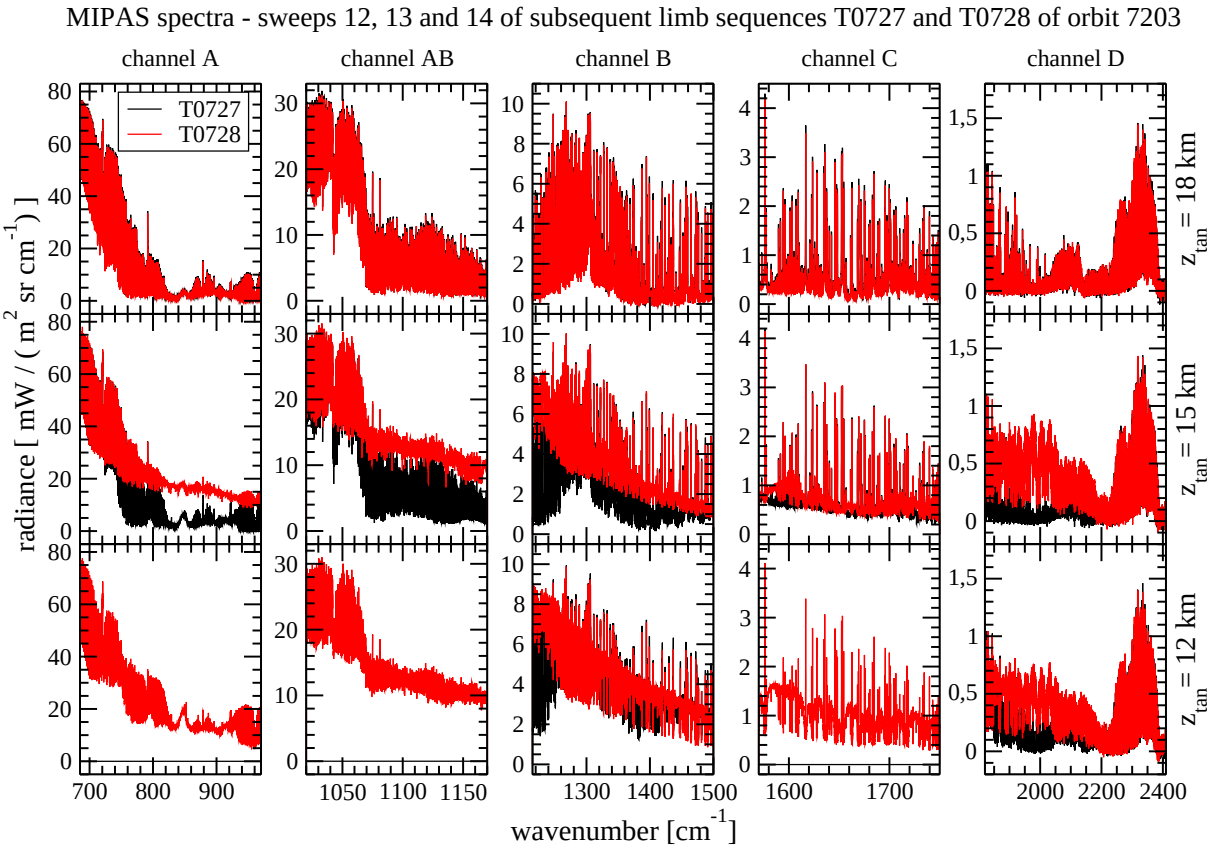

Figure 6.2: *MIPAS spectra of sweep 12 ($z_{\tan} \approx 18\,km$, upper panel), sweep 13 ($z_{\tan} \approx 15\,km$, middle panel) and sweep 14 ($z_{\tan} \approx 12\,km$, lower pannel) of limb sequences T0727 (clear-sky) and T0728 (cloud interfered) of ENVISAT orbit 7203. In sweep 13 spectra of T0728, a significant enhancement of the broadband continuum signal is observed. For T0727 sweep 14 spectral data are missed for channels A, AB and C.*

International Satellite Cloud Climatology Project ISCCP. Nevertheless, high cloud observations by infrared limb emission sounders have become evaluated not until the beginning of the 21st century (Spang et al., 2002a) based on the examination of the strongly increased continuum signal on a low resolution scale.

This broadband intensity enhancement, observable in the atmospheric window regions, is a combined result of the self-emission of the cloud particles and scattering of radiation, primarily originating from the Earth's surface and the troposphere, into the line of sight by cloud particles. Höpfner et al. (2002) have shown, that in case of polar stratospheric clouds (PSC) the previous assumption of neglectable scattering easily fails to model about 15 – 85 % of total radiance in presence of high clouds and results in overestimating cloud extinction coefficients.

Observation and characterization of high clouds by more narrow spectral features like inverted H_2O lines and CO_2 side lobes became of interest along with the operation of instruments with very high spectral resolution like MIPAS. While CO_2 side lobes might as well be caused by a warm cloud observed through colder overlaid atmospheric layers (Spang et al., 2004), H_2O absorption lines can only be explained by a significant amount of upwelling tropospheric ra-

diation scattered into the LOS causing broader tropospheric absorption features superimposed on the stratospheric emission spectrum. Both of these features have been observed in MIPAS measurements and reproduced in simulations for PSC (Höpfner et al., 2002) and cirrus (Ewen et al., 2005) over selected spectral microwindows. However, due to the uncertainty of CO_2 side lobes as well as their minor development in the MIPAS data used here, emphasis is placed on reproducing broadband continuum signal and H_2O absorption features throughout this study.

6.2.2 Placement of Microwindows

Out of the spectral range of MIPAS three microwindows in channels A and B were chosen for validation and cirrus effect study. Similarly to the microwindows used for PSC retrieval from MIPAS-B data by Höpfner (2004), they are located in atmospheric window regions at $825-830\,\mathrm{cm}^{-1}$ (mw1), $947.5-950.5\,\mathrm{cm}^{-1}$ (mw2) and $1224-1228\,\mathrm{cm}^{-1}$ (mw3), covering at least one H_2O line each (see Fig. 6.3). Window mw2, almost only interfered by one H_2O line and two strong CO_2 lines, has as well been used by Ewen et al. (2005) for validation of the Monte Carlo scattering model McClouds_FM and limb measurement of cirrus, and may therefore provide a reference for model capability comparison.

Although the presence of CO_2 side lobes is quite weak in microwindow mw2 of the cloud contaminated spectra of sequence T0728 (Fig. 6.3), this could support a close guess of cloud optical depth and a good measure of having met scattering properties. As can be seen from PSC effect studies in Höpfner et al. (2002) and Höpfner (2004), CO_2 side lobe effects only occur over a certain range of cloud scattering and absorption properties. Furthermore, the microwindow placement over a wider spectral range covering the $830\,\mathrm{cm}^{-1}$ centered ice absorption band (mw1 located in the center, mw2 in the wing and mw3 outside the band) promises for ability to retrieve particle size information.

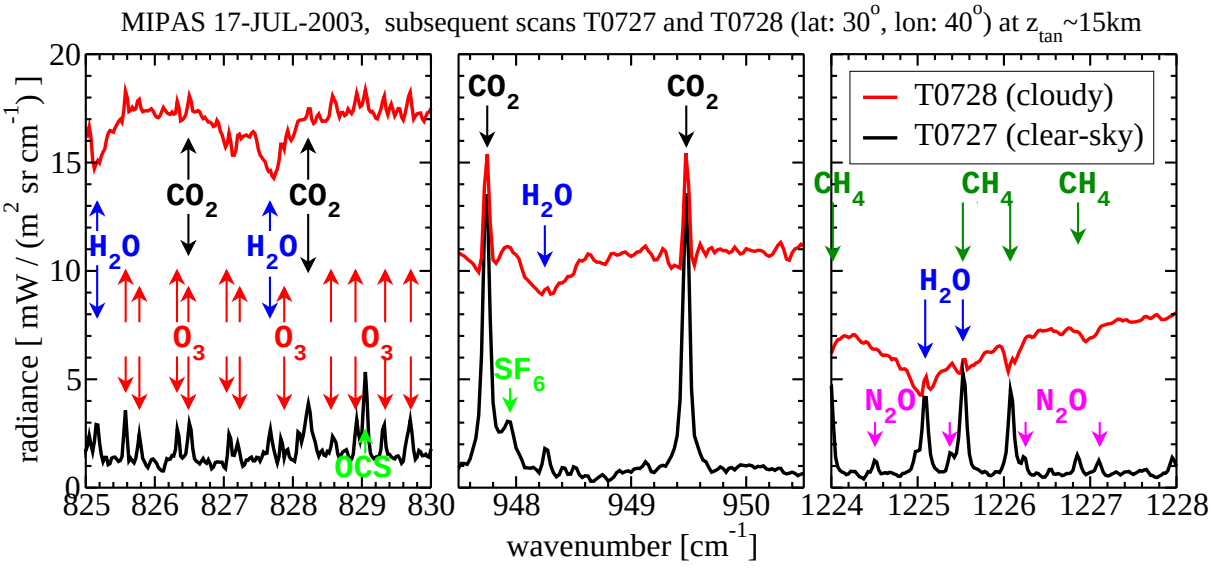

Figure 6.3: *Microwindows used for sensitivity study and cirrus retrieval with sweep 13 spectra of sequences T0727 and T0728. Major interfering trace gases superimposed. The switch of* H_2O *and* CH_4 *from emission lines under clear-sky conditions to broader absorption features in cloud interfered spectra is clearly visible.*

6.2.3 Assumptions in Modeling Ice Clouds

When modeling cloud observations a number of assumptions about cloud properties has been applied implicitly in the radiative transfer model. At present SARTre is only capable of modeling radiative transfer in a one dimensional spherical shell atmosphere. For modeling RT in presence of clouds this implies, that the cloud is spatially contiguous in horizontal direction and consists of uniformely thick and homogeneous layers.

One optional exception from the 1D-assumption is implemented in SARTre (see section 3.3 for more details) by allowing the cloud to exist solely on the observer or the observer-opposite side of the LOS divided by the tangent point (Fig. 3.4). This exception is of crucial importance for modeling limb observations of thin clouds with tangent altitudes below the cloud bottom. In a "fully" 1D-atmosphere the LOS crosses the cloud layer twice – in front and behind the tangent point – with a distance of tens to hundreds of kilometers in between. Both, the cloud part near and the part far of the observer contribute significantly to simulated total limb radiance. But, in "real" atmospheres it is highly implausible to still observe the same cloud or a cloud with similar properties over such distances.

In a spherical shell atmosphere sample path lengths through the layer containing the tangent point become very long, e.g. approximately 200 km through a 1 km thick layer. Using a 1D model, the complete path sample is taken to be clouded. Thus, clouds are assumed to be of larger horizontal extent than the sample length of the LOS through the cloud layer.

Further cloud extent requirements are induced through the instrument's finite field of view (FOV), modeled by simulating and convolving a set of pencil beam observations. While in nature the cloud might cover an arbitrary part of and location in the FOV, it is assumed that the entire FOV is filled by cloud in horizontal (across the line of sight) direction. Concerning vertical FOV, upper pencil beams are allowed to look above the cloud and modeled as clear-sky cases consequentely. Ewen et al. (2005) have shown, that for the entire vertical FOV of MIPAS be filled by the cloud, the horizontal extent of the cloud has to be > 90 km. Both extent requirements can conveniently be considered to be met by a large fraction of cirrus. Cirrus is known to be usually much larger in horizontal than in vertical extent and diverse types of cirrus clouds have frequently been observed with horizontal extents on the order of hundreds of kilometers (Ewen et al., 2005; Kahn et al., 2003). Finally, due to the use of the scattering phase function described in terms of scattering angle, cloud particles are assumed to be randomly oriented.

Some further assumptions in the setup of this study are made in order to limit the number of free parameters in cloud properties. While generally vertical inhomogeneities of the cloud may be taken into account by comprising it of several homogeneous layers, in this study only homogeneous one layer clouds are assumed. Concerning microphysical properties, the cloud is considered to consist of particles of a single crystal habit and to be described by a size distribution representative of the entire cloud body.

6.2.4 Macrophysical, Microphysical and Optical Cloud Properties

Macrophysical Properties

From cloud indices as well as from spectra of the MIPAS sequence T0728 itself, sweep 13 at a tangent altitude of $z_{\tan} \approx 15$ km can be clearly determined as the uppermost measurement "seeing" high clouds. Taking into account the MIPAS field of view, cloud top height z_{top} can be roughly estimated as $14.0\,\text{km} \leq z_{\text{top}} \leq 16.5\,\text{km}$.

Additionally to the assumptions discussed in the previous subsection, for the determination of properties of the cirrus observed in T0728 the subsequent sweeps 13 and 14 are taken to observe the same, homogeneous cloud. When the cloud is only "seen" by a fraction of the instrument's (vertical) FOV, which is likely to happen for upper sweep 13, effects of cloud top height – directly related to the FOV fraction observing the cloud – and cloud optical thickness can hardly be separated (Ewen et al., 2005). Thus, optical thickness will be estimated from sweep 14 spectrum, while cloud top height will then be primarily fitted from sweep 13 spectrum.

Depending on cloud top height and position along the LOS, the assumption of sweep 13 and 14 observing the same cloud requires the cloud to be somewhat larger (up to 400 km) than pointed out before. As mentioned above, cirrus clouds of that extent are not unlikely to be observed. However, the assumption of a homogeneous cloud of that extend is quite rough. It will result in an average estimate of properties of the observed cloud.

Optical Properties

As described in section 3.3 optical properties of clouds have to be provided to SARTre by data files in terms of scattering and absorption coefficients β_s and β_a, respectively, and phase function $P(\Theta)$ of a representative polydispersion. Thus, optical properties of the cloud as a sample of particles have to be calculated externally from single scattering properties of individual particles and microphysical properties of the particle bulk.

Properties of individual particles are extracted from a database of single-scattering properties of non-spherical, randomly oriented particles by Yang et al. (2005). With respect to maximum dimension L, the database lists geometric cross section A, volume V, extinction and absorption efficiency Q_e and Q_a, asymmetry factor g and phase function $P(\Theta)$ at 498 discrete scattering angles Θ of seven ice crystals habits (aggregates, bullet rosettes, solid and hollow columns, plates, droxtals and spheroids). It covers the near through far infrared spectral region, providing properties of each of the crystals at 49 wavelengths between $3-100\,\mu$m for particle sizes ranging from $2-10{,}000\,\mu$m specified in terms of maximum dimension. Single scattering properties were computed from a composite method based on a combination of the finite-difference time-domain technique, the T-matrix method, an improved geometrical-optics method, and Lorentz-Mie theory. Bulk optical properties are derived from single scattering properties as described in chapter 2.3.2.

Microphysical Properties

From various in-situ measurements cirrus clouds of a wide range of particle sizes and size distributions have been reported (e.g. Heymsfield and Platt, 1984; McFarquhar and Heymsfield, 1997; Heymsfield et al., 2002), primarily classified concerning their geographical location and forming mechanism. Since the cirrus observed by MIPAS can neither be clearly assigned to tropical nor midlatitude cirrus and no further investigation has been done on probable forming mechanism, "standard" size distributions have been used.

Two gamma-type distributions (Eq. (2.31)) for cirrus and thin cirrus as used in LOWTRAN and FASCODE have been taken from Shettle (1990). Furthermore, a temperature parameterized size distribution of the form

$$n(a) = A(T)a^{B(T)} \tag{6.1}$$

as given in Liou (1992) and based on Heymsfield and Platt (1984) is used (see Fig. 6.4). Throughout this study, particle size a is described by means of particle maximum dimension L.

None of the used distributions is directly parameterized in terms of particle size. Hence, in order to examine size effects on a wider base, optical properties have been calculated for the full size range as provided by the database of single scattering properties ($2-10000\,\mu$m) and for a limited range of particles sizes between $20-2000\,\mu$m[1]. With a cloud top height above 14.0 km, cloud temperature is expected to be around or below $T=-50\,^{\circ}$C, which has therefore been chosen as parameterization temperature for the Liou size distribution. Distributions for lower temperatures would result in smaller effective particle sizes, but have not been investigated here.

Table 6.1: *Characteristics of size distributions examined in the sensitivity study. Unless otherwise noted, "liou_lim" is used as default distribution. Total number density N and cloud optical thickness τ_c in the three microwindows correspond to temperature parameterized IWC for $T=-50\,^{\circ}C$ as derived from Liou (1992) and cloud geometrical thickness of 1.0 km. Scale denotes a factor to scale IWC and N, respectively, such that τ_c averaged over the microwindows is constant for all distributions.*

name	size range	D_e	N	τ_c			scale
	[μm]	[μm]	[m^{-3}]	mw1	mw2	mw3	
liou_lim	20 – 2,000	36.3	$6.9\cdot10^4$	0.130	0.111	0.137	1.00
liou_full	2 – 10,000	10.5	$2.7\cdot10^7$	0.266	0.152	0.224	0.60
shettle_full	2 – 10,000	41.8	$1.3\cdot10^4$	0.112	0.107	0.111	1.20
shettle_thin_lim	20 – 2,000	9.33	$8.8\cdot10^5$	0.501	0.300	0.659	0.26
shettle_thin_full	2 – 10,000	2.83	$4.4\cdot10^7$	0.939	0.334	0.556	0.20

Cirrus particles usually have non-spherical shape, but often tend to be of regular shape, e.g. hexagonal columns or plates. Predominate shape has been described to vary with vertical position inside the cloud (pristine and small crystals on top, irregular clusters on the cloud bottom) and to depend on humidity and temperature (spatial, polycrystal forms like bullet rosettes at temperatures above $-40\,^{\circ}$C and single crystals, particularily solid and hollow columns, at temperatures below $-50\,^{\circ}$C) (Hallett et al., 2002; Heymsfield and McFarquhar, 2002; Liou, 2002). Due to an expected temperature of the observed cirrus below $-50\,^{\circ}$C, clouds in the study are taken to be composed of solid columns by default, unless the effect of particle shape is studied.

Optical bulk properties calculated from the single scattering property database (Yang et al., 2005) using various size distributions are shown in Fig. 6.4. Ice clouds may furthermore be characterized by the effective size D_e of the polydispersion and its ice water content (IWC). Effective size D_e is defined by

$$D_e \;=\; \int_{L_{min}}^{L_{max}} n(L)\,V(L)\,\mathrm{d}L \;\Big/ \int_{L_{min}}^{L_{max}} n(L)\,A(L)\,\mathrm{d}L\,, \tag{6.2}$$

where $V(L)$ and $A(L)$ denote the volume and geometric cross section, and $n(L)$ is the number density of particles of maximum dimension L. Ice water content, describing the mass of water

[1]The limited range has been chosen according to limitations of the Liou parameterization, which is basically only valid for particles $>20\,\mu$m.

ice contained in a cloud volume, is derived from

$$\mathrm{IWC} \;=\; \rho_i \int_{L_{\min}}^{L_{\max}} n(L)\, V(L)\, \mathrm{d}L, \tag{6.3}$$

where $\rho_i = 0.917\,\mathrm{g/cm^3}$ is the bulk density of ice (Liou, 2002). Ice water path IWP describes the content of ice in the cloud layer of geometrical thickness $\Delta z \;=\; z_{\mathrm{top}} - z_{\mathrm{bottom}}$:

$$\mathrm{IWP} \;=\; \int_{z_{\mathrm{bottom}}}^{z_{\mathrm{top}}} \mathrm{IWC}(z)\, \mathrm{d}z. \tag{6.4}$$

A summary of cloud characteristics is given in Tab. 6.1.

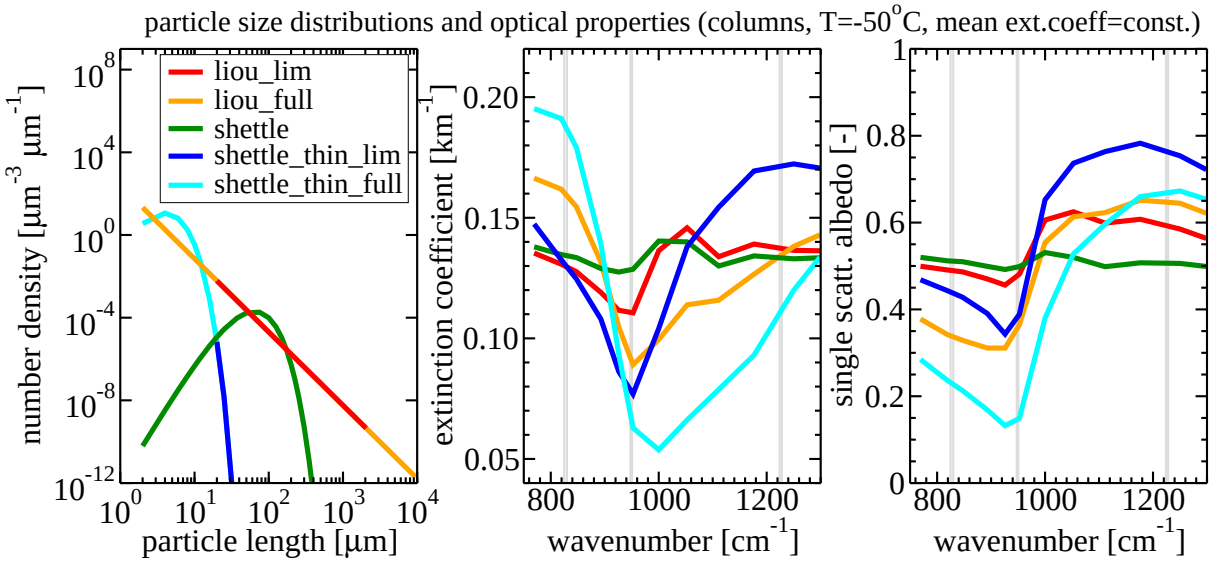

Figure 6.4: *Particle size distributions (left) and resulting optical properties of the polydispersions, represented by extinction coefficients (middle, scaled to a constant mean over the 3 microwindows, see Tab. 6.1) and single scattering albedo (right). Grey vertical lines indicate the positions of the microwindows used in the sensitivity study and derivation of cloud properties.*

6.3 Setup of Atmosphere, Observation Geometry and Sensor

Focused on cirrus cloud effects, other atmospheric conditions, described by temperature, pressure, and gas mixing ratio profiles, have been assumed to be well known and held constant throughout the study. In order to use atmospheric data close to actual conditions, temperature and trace gas profiles retrieved from the MIPAS limb sequences T0728 processed at IMK are used (von Clarmann et al., 2003; Carli et al., 2004). For CO_2, the US standard profile scaled to a base value of 370 ppm is used. Since there is no retrieval carried out from cloud contaminated spectra (defined by a cloud index threshold of 4.5 (Höpfner, 2005)), this approach may cause uncertainties in atmospheric profile data at altitudes below cloud top. However, that means, a priori profile data taken from climatology is used at those altitudes. Pressure profiles have been taken from ECMWF analyses.

MIPAS retrieved profiles, defining the model atmosphere's altitude grid (see section 3.1.3), are given with grid resolution of 1 km between 0 – 44 km and 2 – 10 km resolution above on 64 altitude grid points up to 120 km. Only major contributing molecules have been taken into account (see also Fig. 6.3):

- H_2O, O_3 and CO_2 in microwindows mw1 and mw2,
- H_2O, CH_4, O_3, N_2O and CO_2 in microwindow mw3.

Further trace gases are neglected, although carbonyl sulfide (OCS) and sulfur hexafluoride (SF_6) are found to give strong contributions from single lines at 829.0 cm^{-1} and 947.9 cm^{-1}, respectively (see Fig. 6.3). Water vapor continuum has been taken into account by using CKD continuum data (Clough et al., 1989), extracted from FASCODE (Anderson et al., 1995). Temperature, pressure, and mixing ratio profiles of the trace gases taken into account are shown in Fig. 6.5.

Unlike clear-sky spectra, modeling of cloud influenced limb emission spectra requires knowledge of or assumptions about surface conditions. Examining data measured over Arabian peninsula, the surface is assumed to be of stone or sand desert type. Spectral emissivity was extracted from the ASTER spectral library (Hook, 2005). Although the material originates from the Australian desert, "Desert varnished ferruginous sandstone", the only desert type soil currently listed in the ASTER library, has been decided to be representative for the Arabian desert. Hence, emissivity values are set to 0.96, 0.93 and 0.85 in microwindows mw1, mw2 and mw3, respectively. Surface temperature is set to the temperature of the lowest atmospheric level. Due to missing retrieval results for lower atmospheric layers as well as for potential surface heating of a desert surface at 10:30 am local time, this approach may involve an uncertainty of surface temperature of the order of several K. Although surface emissivity and temperature are not cloud properties, they have been included in the sensitivity study to estimate radiance effects on limb spectra induced by uncertainty of surface conditions.

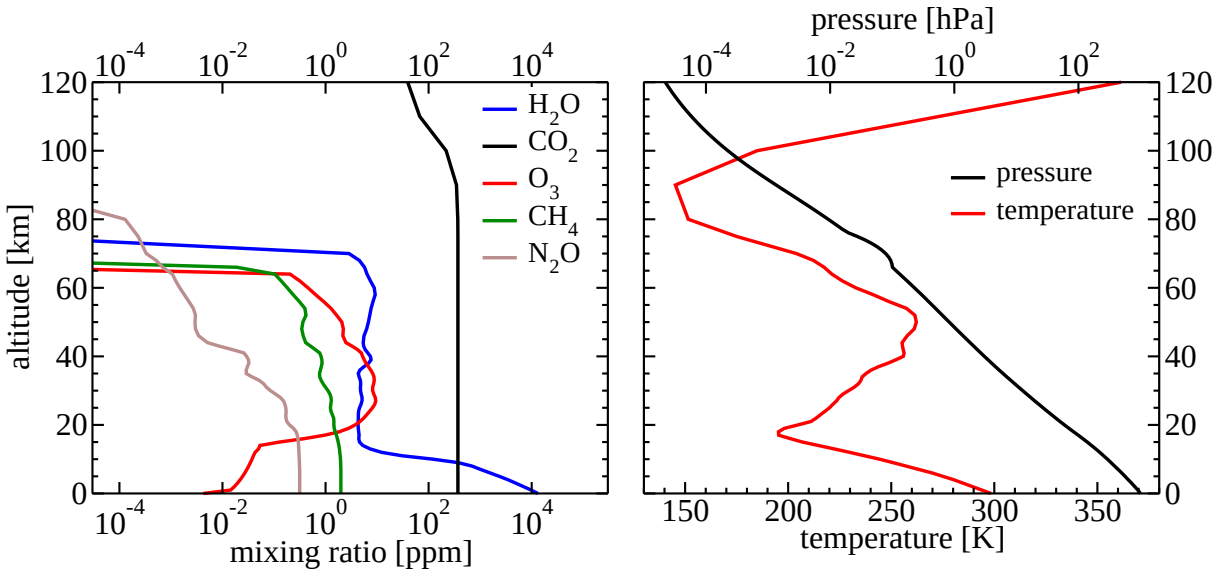

Figure 6.5: *Profiles of trace gas mixing ratios (left) and temperature and pressure (right).*

Geometry of limb observations in a spherical shell atmosphere is fully characterized by observer position z_{obs} and tangent altitude z_{tan}. Observer altitude of $z_{obs} = 786.8\,\text{km}$ is taken from MIPAS Level 1B header data. Since pointing information provided with Level 1B data has an accuracy of only several hundred meters, the use of "true" tangent altitudes resulting from retrieval is more convenient for modeling. However, like atmospheric profiles tangent altitudes are only derived from cloud-free spectra. Thus, for cloud influenced sweeps Level 1B tangent altitudes are corrected by extrapolating the linear fit of differences between Level 1B and retrieved tangent altitudes of the upper, cloud-free observations.

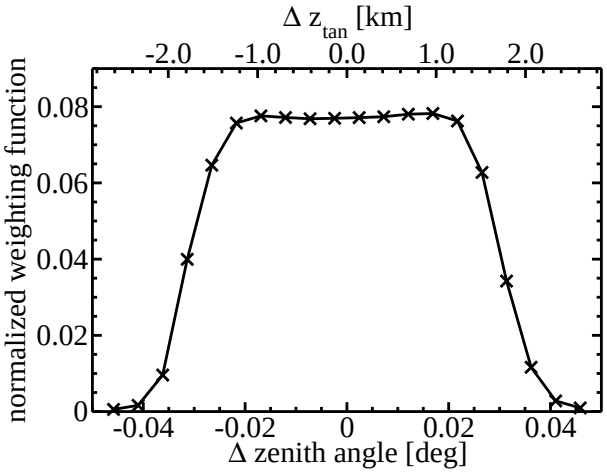

Figure 6.6: *MIPAS field of view function*

The instrument's finite field of view of a width of 0.0917 ° is described by an approximately trapezoidal function of 20 bins that are equidistant in angle (Nett, 2003). In contrast to the nominal FOV of about 3 km in vertical direction as mentioned in section 6.1, the applied FOV is about 5 km wide at tangent point, but with 90 % of the observations weight within 3 km. The FOV function is shown in Fig. 6.6. Tab. 6.2 presents a summary of observation geometry characteristics of examined sweeps 12 – 14 of limb sequence T0728.

Finally, for comparison of measured and modeled spectra, spectrally very high resolved simulation resulting from monochromatic line-by-line calculations have to be convolved with instrumental line shape (ILS) and interpolated to MIPAS spectral grid with $0.025\,\text{cm}^{-1}$ spacing. In order to avoid artefacts from ILS of Fourier Transform Spectrometer instrument in the spectra, which might mistakenly be accounted for scattering features, strong apodization (Norton and Beer, 1976) is applied on both measured and modeled spectra. The complete post processing, including field of view and instrumental line shape convolutions, is carried out independently of the SARTre model.

Table 6.2: *Summary of observational geometry characteristics*

sweep	Level 1B z_{tan}	retrieved z_{tan}	corrected z_{tan}	FOV	(90 %)
12	18.035	17.746	—	15.16 – 20.33	(16.25 – 19.24)
13	15.125	—	14.950	12.36 – 17.54	(13.45 – 16.45)
14	12.220	—	12.070	9.48 – 14.66	(10.57 – 13.57)

6.4 Sensitivity Study

In order to examine effects of diverse cirrus cloud parameters on infrared limb spectra and to derive estimates of properties of the observed cirrus cloud in MIPAS sequence T0728, a sensitivity study is carried out. Effects of cloud properties ice water path IWP or cloud optical thickness τ_c, respectively, cloud top height z_{top} and geometrical thickness Δz, effective particle size D_e or size distribution, crystal habit and cloud position are studied. Furthermore, effects of varied tangent altitude and surface properties (temperature and emissivity) are examined to check deviations, that might be caused by uncertainties of these parameters.

Due to the difficulties concerning FOV filling of sweep 13, as discussed in 6.2.4, sensitivity study is done with observation geometry parameters of sweep 14 and in comparison to the sweep 14 MIPAS measurement. Furthermore, all parameters are examined using spectra convolved with the MIPAS FOV function, except for crystal habit and surface properties, where pencil beam simulations are used.

Of the parameters under investigation, ice water path and cloud optical thickness, respectively, are those that cause the largest variability in the spectra. Therefore, these parameters are the first to be estimated. The sensitivity study of other parameters is continued with optical thickness and/or ice water path fixed to the estimated value. Being directly related to broadband continuum signal, cloud optical thickness τ_c is used as the reference parameter. While ice water path and optical thickness are closely linked, their relation in the infrared spectral region highly depends on size distribution and crystal habit, meaning a certain IWP may translate to a wide range of optical thickness and vice versa. Therefore, effects of particle size and shape are studied separately for fixed IWP and fixed τ_c.

Table 6.3: *Parameters of cirrus clouds and observation conditions examined. For studying sensitivity concerning single parameters, other parameters are fixed on default values.*

parameter	default value	variation range
optical thickness τ_c	0.005	0.002 – 0.1
top height z_{top}	16.45 km	12.95 – 16.45 km
geometrical thickness Δz	1.0 km	0.1 – 2.5 km
cloud position	whole layer	whole layer, in front, behind of tangent point
size distribution	liou_lim	see Tab. 6.1
crystal habit	solid columns	aggregates, solid and hollow columns, droxtals, plates, bullet rosettes
tangent altitude z_{tan}	14.95 km	14.45 – 15.45 km
surface emissivity ε_{surf}	0.96 / 0.93 / 0.85	0.90 – 1.00 / 0.90 – 1.00 / 0.80 – 0.95
surface temperature T_{surf}	298 K	286 – 310 K

6.4.1 Cloud Optical Thickness

To get a first estimate of τ_c, calculations for $0.002 \leq \tau_c \leq 0.1$ covering subvisible to thin cirrus, were performed. All other parameters were fixed at default values given in Tab. 6.3. Resulting spectra are shown in Fig. 6.7.

For the subvisible to thin clouds investigated here, a successive increase of the continuum signal with increasing cloud optical thickness is observed. Water vapor absorption features are found to occur for $\tau_c \geq 0.005$ in form of side lobe features first and as inverse H_2O lines for $\tau_c \geq 0.01$. The spectral behavior in microwindow mw3 is somewhat different, due to higher interference of trace gas contributions. Nevertheless we can observe the spectra switching from emission to absorption type spectra when the cloud becomes thicker. Clear absorption features are not only observed for water vapor, but also for methane (CH_4), which has a similar vertical distribution of mixing ratio (see Fig. 6.5).

From comparing simulation results to the MIPAS spectra, cloud optical thickness can roughly be estimated as $\tau_c \simeq 0.005$. Corresponding spectra fit the measurement well at microwindows mw1 and mw2 concerning both, the broadband continuum signal and the water vapor spectral features, that occur only as side lobes at MIPAS sweep 14. While finer spectral features of simulated spectra with $\tau_c \simeq 0.005$ in mw3 as well match the ones observed in MIPAS data, the continuum signal is underestimated by about 25 %. From broadband continuum in mw3 alone, optical thickness of $\tau_c \simeq 0.008$ would be estimated.

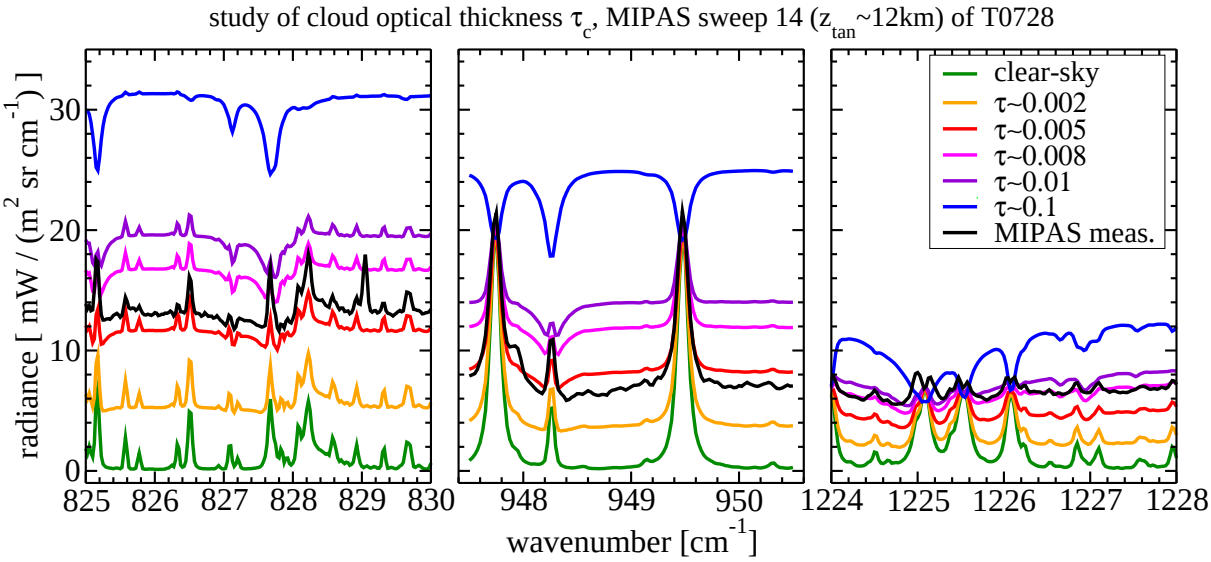

Figure 6.7: *Sensitivity to cloud optical thickness τ_c variations for subvisible and thin cirrus.*

However, unless otherwise noted the following studies are done with cloud optical thickness fixed to $\tau_c \simeq 0.005$, which corresponds to IWP $= 0.1\,\mathrm{g/m^2}$ and total particle number density $N = 3.8 \cdot 10^3\,\mathrm{m^{-3}}$ for the default size distribution ("liou_lim") and crystal habit (solid columns). Concerning deviating estimates of τ_c from mw1/mw2 and mw3, effects of other parameters will be examined to their ability to homogenize optical thickness estimate. Beside, it has to be noted, that significant changes in τ_c might influence the effects of other parameters on spectral intensity to a great extent.

6.4.2 Cloud Top Height

Effects of varied cloud top height are examined, shifting z_{top} from default value 16.45 km down to 12.95 km in steps of 0.5 km with all other parameters including cloud geometrical thickness Δz fixed on default values. Results are shown in Fig. 6.8.

Over all microwindows, decreasing cloud top height causes an increased continuum signal for $z_{\text{top}} \geq 13.95$ km. Effects are similar to those, that can be expected for increasing cloud optical thickness by some percent. But, differences are found concerning spectral features resulting from contributions of above the cloud. E.g. emission peaks in the center of the water vapor lines at 828.7 cm^{-1} and 948.3 cm^{-1} are more pronounced. Decreasing z_{top} below 13.95 km then leads to a decreasing continuum signal.

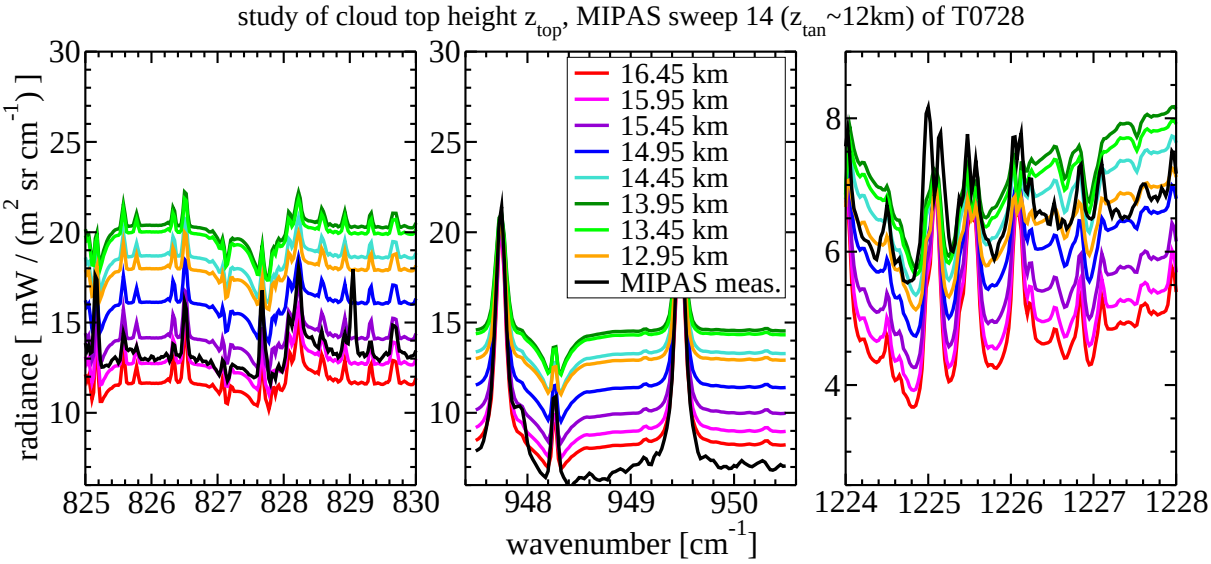

Figure 6.8: *Sensitivity to varying cloud top height* z_{top}

This behavior can mainly be explained by a change of the amount of emitting and scattering cloud particles observed by the instrument, integrated over the line of sight and the field of view. With the complete vertical FOV "looking" below the cloud, as for sweep 14 with $z_{\text{tan}} \approx 12$ km and the cloud located between 15.45 – 16.45 km altitude, shifting the cloud down increases line of sight path lengths through the cloud. That means, observed cloud mass is increased, which causes an enhancement of the cloud response and, thus, of the continuum signal of the top-of-atmosphere spectra. Cloud path length of a pencil beam is largest, when the tangent point of the line of sight (LOS) meets the bottom of the cloud. Shifting the cloud further down that point decreases cloud path length again, resulting in decreasing continuum signals. This effect is strengthened, when the upper part of the FOV does not observe the cloud anymore but the upper clear-sky atmosphere, which gives a very low broadband contribution in comparison to the cloud.

A further reason for increased continuum signal might be that a lower tropospheric cloud is generally a warmer cloud, thus emitting more radiation. On the other hand, this effect could be balanced by a higher cloud extinction below the LOS, allowing less radiation from the surface to penetrate to the scattering points along the line of sight. However, the largest effect is expected to be caused by varying cloud path length, i.e. by varying the integrated optical thickness of the cloud along the LOS.

6.4.3 Cloud Geometrical Thickness

For studying effects of cloud geometrical thickness, Δz is varied between 0.1 and 2.5 km. Total optical thickness of the cloud and ice water path, respectively, are fixed, i.e. ice water content is varied by a factor of 10.0 to 0.4 regarding the default case with $\Delta z = 1.0$ km. Other parameters including cloud top height are fixed as well. Fig. 6.9 presents results of the simulations.

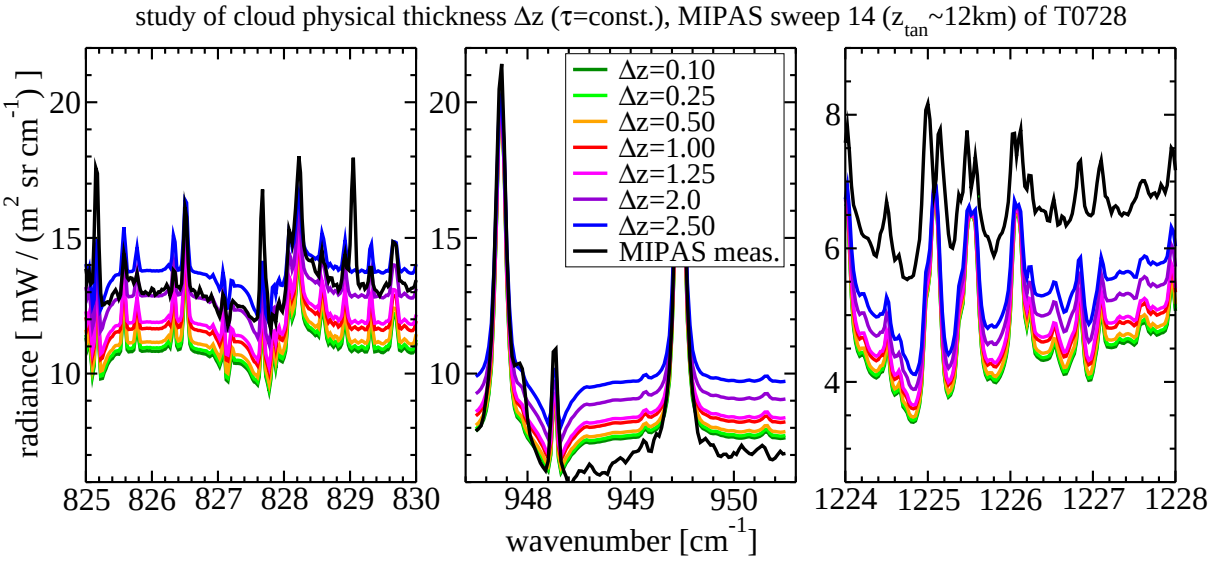

Figure 6.9: *Sensitivity to variations in cloud geometrical thickness* Δz

Except for the centers of the strong lines, changing the geometrical thickness of the cloud generally causes almost constant offsets, with increasing Δz leading to an increase of the signal. The signal is almost insensitive to changes of geometrically thin clouds. Thickening the cloud by a factor of 5 from 0.1 to 0.5 km results in an intensity offset $< 0.3\,\mathrm{mW/(m^2\,sr\,cm^{-1})}$, while a further thickening by a factor of 5 to $\Delta z = 2.5$ km causes offsets of about $1.0\,\mathrm{mW/(m^2\,sr\,cm^{-1})}$ (mw3) to $2.6\,\mathrm{mW/(m^2\,sr\,cm^{-1})}$ (mw1).

Although cloud path lengths differ a lot for clouds of varied geometrical thickness, the observed emitting and scattering cloud mass is almost constant. The signal enhancement for geometrically thicker clouds with a fixed cloud top rather results from the thicker clouds reaching down to lower and warmer parts of the troposphere. Thus, the cloud emits more radiation directly into the LOS direction and scatters radiation of enhanced intensity from warmer cloud parts into the LOS as well. This explanation matches the finding, that increasing cloud thickness from 0.5 km to 2.5 km causes much larger enhancements than the thickening from 0.1 km to 0.5 km. With temperature changing almost linearly with altitude (see Fig. 6.4), cloud bottom temperature changes significantly from $\Delta z = 0.5$ km to $\Delta z = 2.5$ km (by ≈ 15 K), but varies only slightly from $\Delta z = 0.1$ km to $\Delta z = 0.5$ km (by ≈ 2.5 K).

6.4.4 Particle Size Distribution

Apart from the default size distribution "liou_lim", effects of other size distribution parameterizations and particle size limits are studied in this subsection. Characteristics of resulting polydispersions are given in Tab. 6.1. As can be seen there, both using another size distribution parameterization as well as changing the particle size limits, over which the parameterization is applied, results in different effective particle sizes of the bulk.

Furthermore, for constant ice water path the optical thickness of the clouds varies greatly. Between the microwindows, cloud extinction coefficients and optical thickness, respectively, as well as cloud single scattering albedo differ significantly for different size distributions (see Fig. 6.4). Due to a different weighting of small and large particles, distributions having similar effective particle sizes of the polydispersions do not necessarily result in similar optical properties (for that compare "liou_full" and "shettle_thin_lim"). However, distributions with small effective sizes cause distinct gradients in both extinction and single scattering albedo around $900-1000\,\mathrm{cm}^{-1}$ that vanish for larger sizes.

Deviating radiative properties, that will result from different bulk optical properties, should allow for retrieving information about particle size or size distribution. In particular, fitting a proper particle size is expected to correct for a significant part of deviations left after fitting optical thickness (see subsection 6.4.1).

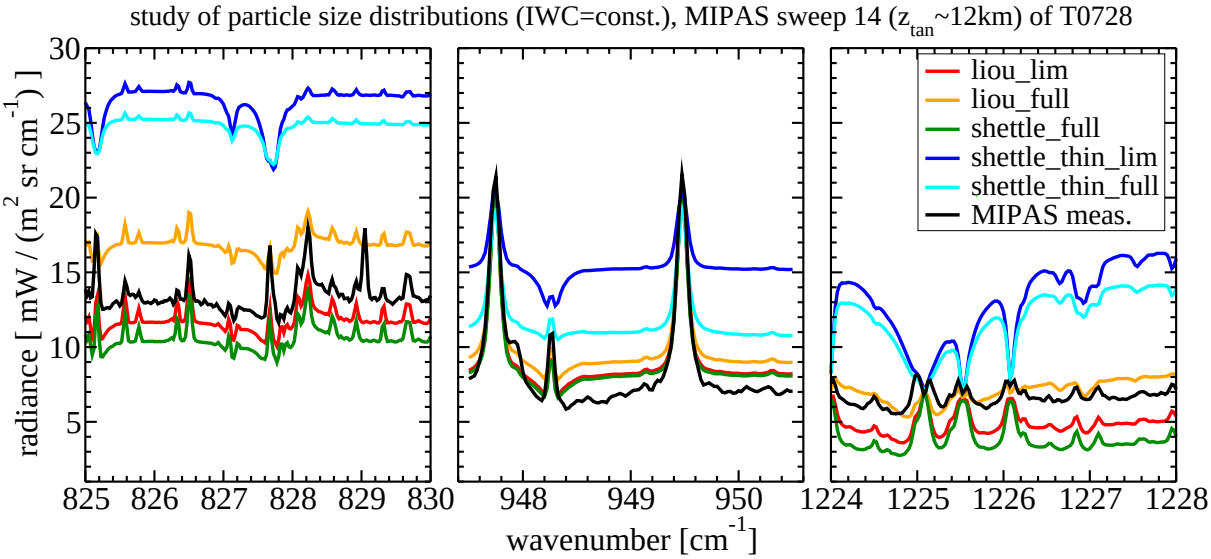

Figure 6.10: *Sensitivity to particle size and size distribution with* IWC $= 1.0 \cdot 10^{-4}\ g/m^3$ *for all distributions*

Results of varied particle size distribution with fixed IWC are shown in Fig. 6.10. At all 3 microwindows, the smallest broadband continuum signal is observed for "shettle_full" distribution, followed by "liou_lim" and "liou_full". Largest signals are found for the thin cirrus distributions from Shettle (1990), "shettle_thin_full" and "shettle_thin_lim". When comparing to Tab. 6.1, a close relation between cloud optical thickness and broadband signal becomes obvious. Beside that, for distribution "shettle_thin_full", characterized by a very small effective size ($D_e = 2.8\,\mu$m), water vapor absorption features in microwindows mw1 and mw2 are much weaker than for other distributions with comparable or smaller continuum signals. With inverse

H_2O lines being caused by scattering of radiation into the LOS, weaker absorption features correspond to the low single scattering albedos for "shettle_thin_full" in mw1 and mw2, which are characteristic for polydispersions of very small particles, i.e. of particles with low size parameter (see subsection 2.3.2).

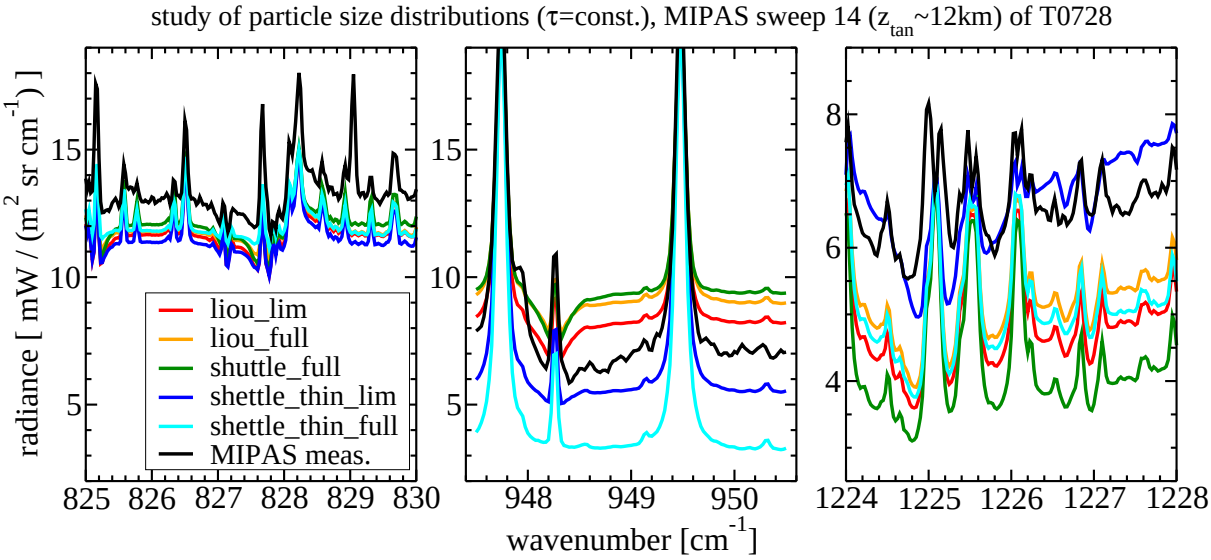

Figure 6.11: *Sensitivity to particle size and size distribution with mean $\tau_c \approx 0.005$ for all distributions*

To examine effects of size distributions apart from dominating optical thickness variation, IWC of the distributions has been rescaled, such that mean optical thickness over the microwindows is constant for all distributions. Scaling factors are listed in Tab. 6.1. Results for varied size distribution with fixed cloud optical thickness are presented in Fig. 6.11.

Compared to spectra for clouds of constant IWC (Fig. 6.10), the variation of the continuum signal is much smaller for fixed mean optical thickness, especially in microwindows mw1 and mw3. As shown in Fig. 6.4, examined size distributions cause different spectral behavior of the cloud optical properties. For fixed mean τ_c this can be found in the spectra as well, where a different relative behavior of the broadband response can be observed. For example, the "shettle_full" distribution gives the highest continuum intensity of all examined distributions in microwindows mw1 and mw2, but the lowest in mw3. On the other hand, "shettle_thin_lim" has the lowest continuum signal in microwindow mw1, a rather low in mw2, but a much higher response than all other distributions in mw3.

Similar to the examined spectra with constant IWC of the cloud, water vapor absorption features in microwindows mw1 and mw2 almost vanish for "shettle_thin_full" distribution with very small effective size. From comparing spectra of "liou_full" and "shettle_thin_lim", for which polydispersions have similar effective particle sizes D_e, it becomes obvious that D_e does not sufficiently describe the relation between particle sizes in a polydispersion on the one and optical or radiative properties on the other hand. However, by simultaneously using several microwindows for the retrieval of cirrus properties, more comprehensive information about size distribution may be derived.

6.4.5 Crystal Habit

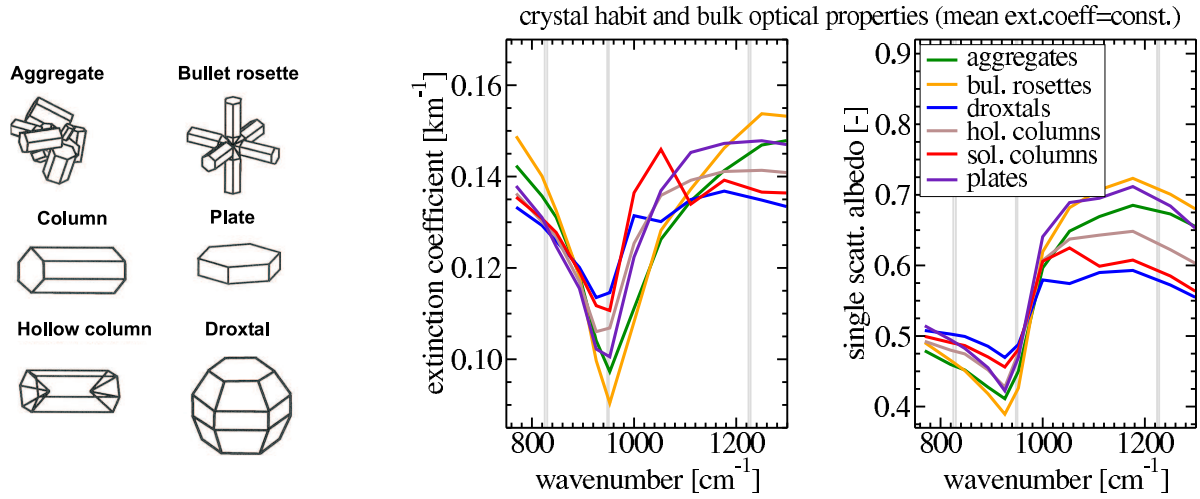

Figure 6.12: *Bulk optical properties, represented by extinction coefficients (left, scaled to constant mean, see Tab. 6.4) and single scattering albedo of the polydispersion, resulting from different crystal habit*

Ice clouds usually consist of non-spherical particles. Often particles are regular crystals, but especially for larger particles irregular shapes (e.g. aggregates, clusters of crystals) occur as well. Crystal habit has been observed to depend on parameters like temperature, humidity, forming mechanism, and age of the ice cloud and usually varies inside the cloud. That introduces a number of free parameters into modeling of cloud interfered spectra and retrieval of cloud properties, respectively. Within this study only homogeneous clouds consisting of single shaped, randomly orientated particles are taken into account. The effects of different crystal habits, for which single scattering properties are provided by the database of Yang et al. (2005), are investigated.

Table 6.4: *Characteristics of polydispersions with varied crystal habit. Total number density N and cloud optical thickness τ_c in the three microwindows refer to temperature parameterized IWC for $T = -50\,°C$ as derived from Liou (1992) and cloud geometrical thickness of 1.0 km. Scale denotes a factor to scale IWC and N, respectively, such that τ_c averaged over the microwindows is constant for all particle shapes.*

crystal habit	D_e	N	τ_c			scale
	[μm]	[m^{-3}]	mw1	mw2	mw3	
aggregates	47.6	$8.3 \cdot 10^4$	0.087	0.063	0.094	1.55
bullet rosettes	18.0	$1.8 \cdot 10^5$	0.246	0.164	0.270	0.56
droxtals	13.5	$1.5 \cdot 10^4$	0.036	0.032	0.038	3.55
hollow columns	30.3	$8.2 \cdot 10^4$	0.146	0.119	0.157	0.90
solid columns	36.3	$6.9 \cdot 10^4$	0.130	0.111	0.137	1.00
plates	25.5	$1.2 \cdot 10^5$	0.177	0.138	0.202	0.73

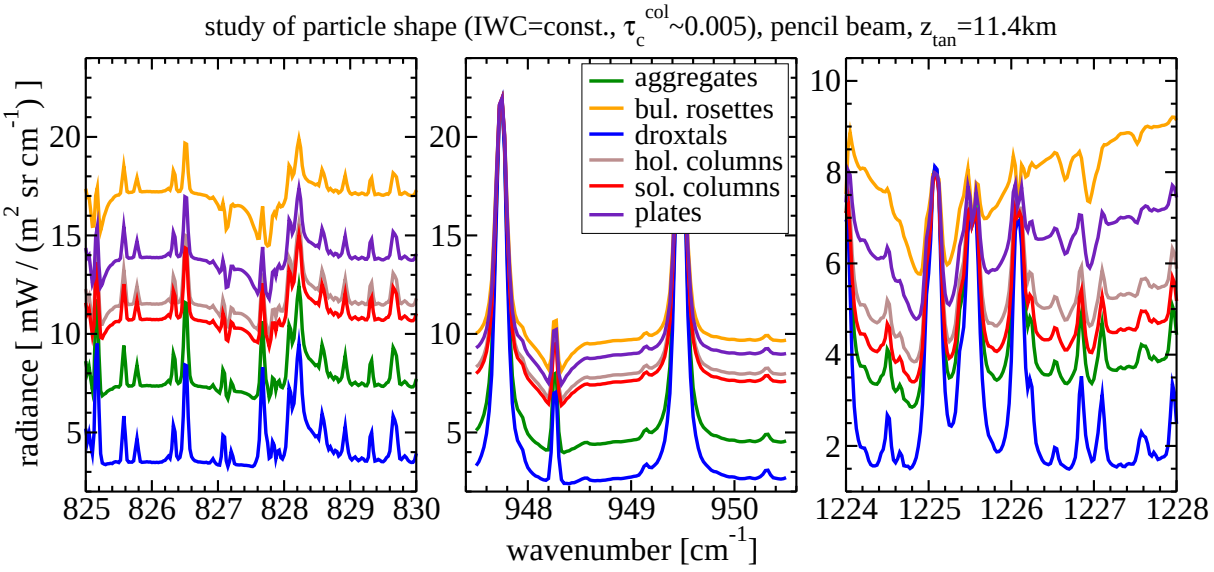

Figure 6.13: *Sensitivity to particle shape with* IWC $= 1.0 \cdot 10^{-4}\ g/m^3$ *(subvisible cirrus) for all distributions*

Similarly to the implementation of different size distributions, the question of fixed reference parameter arises with the use of different crystal habits. When changing the crystal habit, ice water content, optical properties, particularly extinction coefficient, and effective size of a given distribution vary intrinsically. Out of these, crystal habit effects for constant IWC and constant mean extinction coefficient (or cloud optical thickness) over the three microwindows are examined, using the default size distribution "liou_lim". Cloud macrophysical properties are fixed on the values given in Tab. 6.3. Tab. 6.4 lists the cloud characteristics for the investigated crystal habits with IWC fixed. Since instrumental FOV can be considered to have no effect in studying crystal habit, pencil beam spectra ($z_{\tan} = 11.4\,\mathrm{km}$) are calculated.

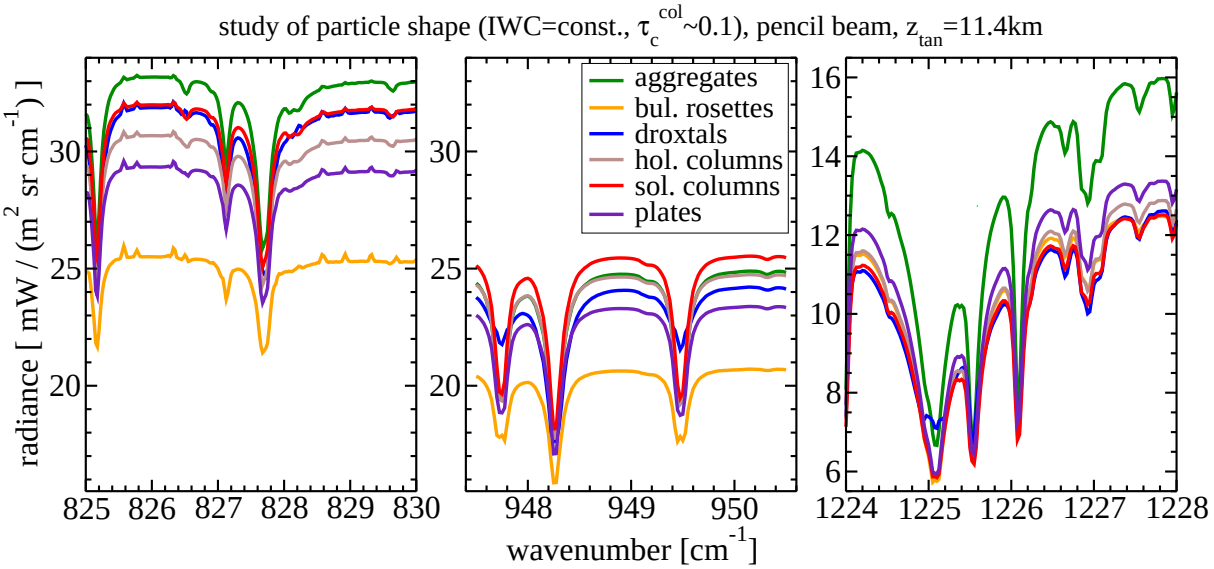

Figure 6.14: *Sensitivity to particle shape with* IWC $= 2.1 \cdot 10^{-3}\ g/m^3$ *(thin cirrus) for all distributions*

Results for clouds with different crystal habit, but fixed ice water content of $\mathrm{IWC} = 0.1 \cdot 10^{-3}\,\mathrm{g/m^3}$ are shown in Fig. 6.13. Different crystal habits are found to have a similar relative behavior to each other in all of the 3 microwindows. Bullet rosettes are observed to cause the largest increase of the continuum signal, while droxtals lead to a rather low enhancement. Comparing these findings to the cloud characteristics presented in Tab. 6.4, it becomes obvious, that these results are mainly caused by varying cloud optical thickness. At all 3 microwindows, a cloud formed by droxtals has the lowest and one of bullet rosettes gives the largest optical thickness, when IWC is fixed, with all the other crystal habits lined up in between in the same order as in Fig. 6.13.

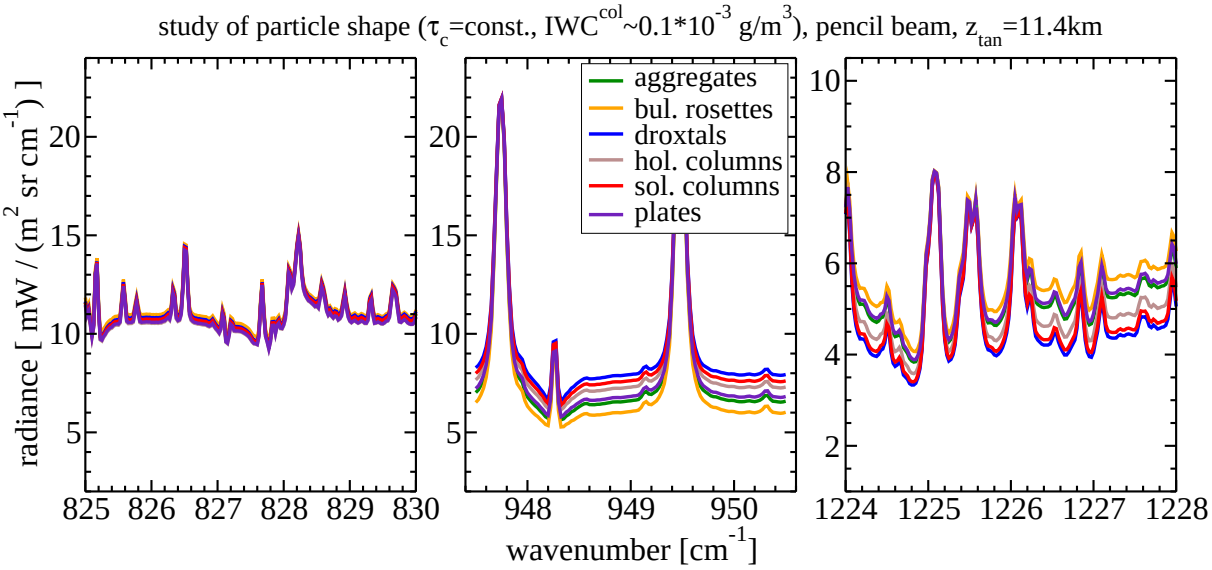

Figure 6.15: *Sensitivity to particle shape with mean $\tau_c \approx 0.005$ (subvisible cirrus) for all distributions*

When examining crystal habit effects for clouds of larger IWC, another behavior is observed. Fig. 6.14 presents resulting spectra for cirrus clouds of $\mathrm{IWC} = 2.1 \cdot 10^{-3}\,\mathrm{g/m^3}$, the nominal IWC that results from the parameterization of Liou (1992) for $T = -50\,^{\circ}\mathrm{C}$. Following the definition of Sassen and Cho (1992), all clouds are subvisible for $\mathrm{IWC} = 0.1 \cdot 10^{-3}\,\mathrm{g/m^3}$, while those of $\mathrm{IWC} = 2.1 \cdot 10^{-3}\,\mathrm{g/m^3}$ span the range from thick subvisible (droxtals) to thin moderate (bullet rosettes) clouds. According to Emde (2005), the enhancement of the broadband continuum signal in the mid-IR reaches a peak, when the cloud becomes opaque in limb but is still transparent in nadir direction. That happens when the ice cloud is thin to moderate, i.e. over the range of cloud optical thicknesses held by the clouds studied here. For thicker clouds, continuum signal decreases and spectral features resulting from scattered radiation (H_2O absorption features and CO_2 side lobes) are less pronounced or even disappear. This effect can be observed for clouds formed by bullet rosettes, plates, hollow and solid columns, while it can be assumed, that aggregates and droxtals have not reached the peak of continuum enhancement yet.

Beside that, it can be found, that spectra for clouds of larger IWC behave slightly different in the microwindow mw3 in relation to mw1 and mw2. Furthermore, deviations between solid and hollow columns, that are small for clouds of small IWC and optical thickness, become more pronounced for thicker clouds. In conclusion, a decreasing sensitivity with respect to IWC and

cloud optical thickness, respectively, when clouds become thicker is accompanied by a higher sensitivity to particle shape.

However, similar to the size distribution study, the observed behavior of spectra from clouds of different crystal habits but fixed IWC, is rather caused by deviating cloud optical thickness than by crystal habit. Therefore, effects of different particle shapes of clouds of fixed mean optical thickness are studied in addition. Results are shown in Fig. 6.15 ($\tau_c \approx 0.005$) and Fig. 6.16 ($\tau_c \approx 0.1$). As expected, spectral deviations due to different crystal habit are much smaller for fixed optical thickness than for fixed IWC. Nevertheless, it can be found that the continuum signal is still correlated with the cloud optical thickness in each of the microwindows. But, from the different relations of $\tau_c^{mw1} : \tau_c^{mw2} : \tau_c^{mw3}$ for different crystal habit, information about particle shape may be estimated.

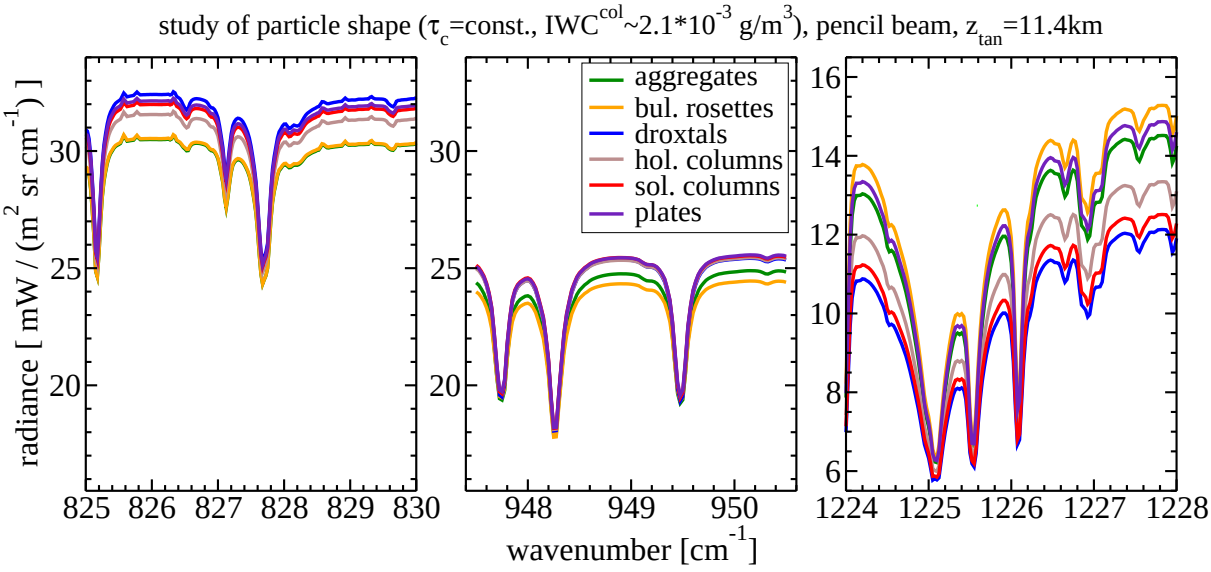

Figure 6.16: *Sensitivity to particle shape with mean $\tau_c \approx 0.1$ (thin cirrus) for all distributions*

Yang et al. (2005) have furthermore shown, that optical properties are very similar for particles of different crystal habit but same effective size of the single particles. This should also apply for radiance spectra. For studying that, size distributions would have to be applied in terms of effective single particle size instead of maximum dimension. Then, different effective bulk size than crystal habit would be derived. But, from additional retrieving optical thickness in each microwindow, ice water content and effective size together, educing about crystal habit or at least compactness of particles could be possible. However, that requires more detailed studies.

6.4.6 Cloud Extent and Position

Basically, simulating radiative transfer in a spherical shell atmosphere means, that a cloud layer is covering the complete spherical shell all over the planet. A line of sight pointing below the cloud layer intersects this layer twice. When the atmosphere along the LOS is transparent between the observer and the observer-far cloud intersection point, i.e. when the total optical thickness (molecular and cloud optical thickness) along the LOS is ≤ 1, a strong signal originating from

the far part of the cloud can be observed. That is always the case for thin cirrus clouds observed in an atmospheric window. But, in reality most clouds do not have such a large horizontal extent (in the order of several hundreds of kilometers), at least they are far from being homogeneous over such large ranges. Therefore, a one dimensional RT model will usually tend to overestimate radiances compared to the "true" signal of the cloud.

As explained in chapter 3, SARTre offers the option to have a cloud placed only on the observer or the observer-opposite side of the tangent point, such that the LOS intersects the cloud only once. Here, effects due to the cloud position in front or behind the tangent point or over the whole layer are studied. When placing a cloud with default properties in front or behind the tangent point, the total amount of observed cloud mass would be approximately half of the one for a whole layer cloud. To study effects of differently placed clouds with approximately the same observed cloud mass as well, cases with doubled ice water content of the cloud are examined as well. Results are shown in Fig. 6.17.

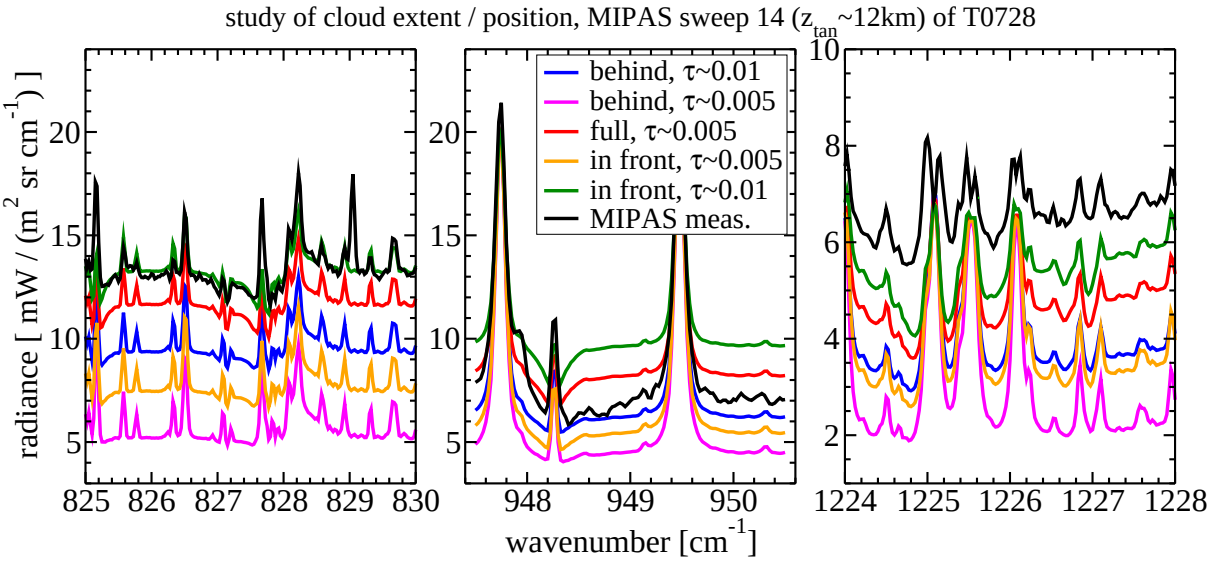

Figure 6.17: *Sensitivity to variations in position/extent of subvisible clouds*

From Fig. 6.17 it becomes evident, that the same subvisible cloud placed on only one side of the tangent point instead of over the whole layer, gives a much lower signal at all microwindows. As mentioned before, this results from less cloud mass being observed by the instrument. Similar to the observation of a thinner cloud, water vapor absorption features are less pronounced. Comparing the responses of clouds in front to those located behind the tangent point, clouds on the observer side are found to have a significantly larger continuum signal. This is simply because the transmission of the cloud signal from the observer-far side to the observer is smaller than that from the observer side due to a longer path through the atmosphere.

When doubling the IWC of the one side clouds, such that the observed cloud mass is approximately the same as for the default cloud covering the whole layer, the response of the default cloud is just between those of the one side located ones. A cloud of doubled IWC in front of the tangent point gives the largest continuum signal at all microwindows. However, changes in the spectrum can hardly be separated from effects of varied IWP or optical thickness, respectively.

6.4.7 Tangent Altitude

Although not a cloud property, effects of varied tangent altitude are studied, in order to check deviations, that are introduced by uncertainty of the tangent altitude and which might influence retrieved cloud properties. Tangent altitudes from MIPAS pointing information have an accuracy of about 1.5 km only. Uncertainty of tangent altitudes derived from MIPAS retrievals is ≈ 200 m (von Clarmann et al., 2003), but no retrievals are done for cloud interfered tangent altitudes. Nevertheless, accuracy of tangent heights derived from a linear extrapolation of differences between pointing information altitudes and retrieved ones, should be better than that of altitudes from pointing information alone. Hence, tangent altitude is varied by up to ± 0.5 km of the default tangent height of 12.07 km for sweep 14. Results are presented in Fig. 6.18.

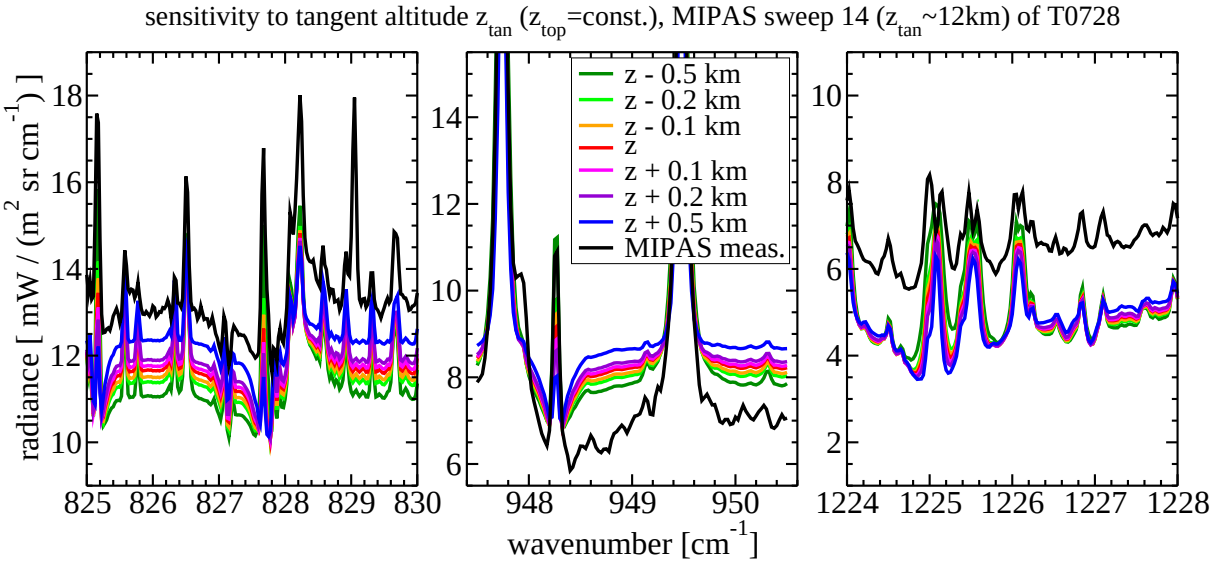

Figure 6.18: *Sensitivity to uncertainties in tangent altitude $z_{\tan}$ with $z_{\text{top}} = 16.45$ km for all tangent altitudes*

Increasing tangent altitude results in an increase of the broadband continuum signal in all 3 microwindows. For a LOS pointing below the cloud, shifting the tangent point up leads to longer path lengths through the cloud and thus, to a higher signal. Nevertheless, signal changes are rather low, particularly in the microwindow mw3, compared to those introduced by an equivalent shift of cloud vertical position (see subsection 6.4.2). Furthermore, unique features are found around the strong H_2O lines at 827.7 cm^{-1} and 1225.0 cm^{-1}. Unlike the continuum signal, the intensity at the flanks of the 827.7 cm^{-1} line stays constant and the intensity in the line center even decreases with increasing tangent altitude. A similar behavior is observed for the 1225 cm^{-1} line, but with a decreasing intensity also in the off center region. This is due to the signal at the strong water vapor lines resulting from molecular emission only, which is stronger at higher temperatures and for higher H_2O content.

Much of the effect of a tangent altitude variation is assumed to be dedicated to the shift relative to the cloud. Thus, uncertainties of the tangent altitude might directly translate to uncertainties in vertical cloud position. To validate this assumption, effects of a combined shift of tangent altitude and vertical cloud position are investigated with shifts of the same value as those for tangent altitude alone. Results are shown in Fig. 6.19.

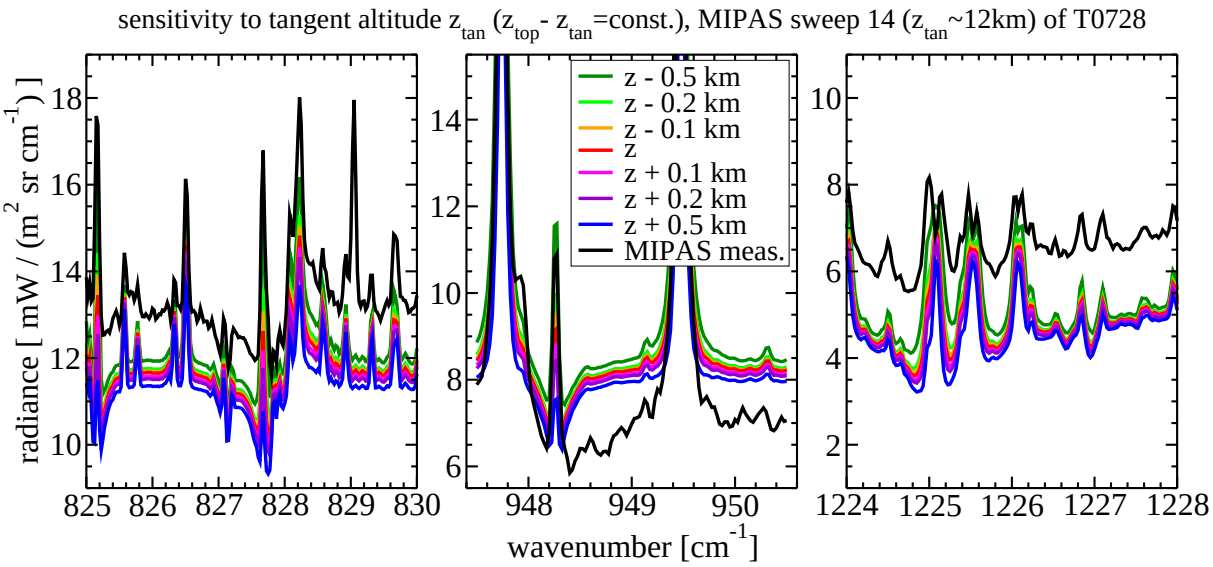

Figure 6.19: *Sensitivity to uncertainties in tangent altitude* $z_{\tan}$ *with* $z_{\text{top}} - z_{\tan} \approx 4.4\,km$ *for all tangent altitudes*

Changes in the spectra are indeed found to be significantly lower, when tangent altitude is varied in combination with z_{top}. While shifting the cloud up results in a lower broadband signal, increasing tangent altitude causes higher signals. Thus, when varying them in combination the effects nearly cancel each other out. The cloud shifting effect is somewhat larger. Hence, increasing the parameters together results in slightly decreasing continuum signal. However, largest deviations are those around the water vapor lines, which are due to varied tangent altitude. From that it might be possible to retrieve tangent altitudes for cloud interfered spectra independently of cloud top height. On the other hand, high variability of temporal and spatial distribution of water vapor complicates that task.

6.4.8 Surface Temperature and Emissivity

Observing thin and subvisible cirrus at midlatitude or tropical latitudes, the broadband continuum signal in the atmospheric window regions is significantly enhanced compared to clear-sky observations. By far the largest fraction of enhancement results from radiation originating from the surface scattered into the LOS. Hence, surface properties, particularly surface temperature and emissivity, may influence cloud observation measurements to a great extent.

Although surface emissivity in the mid-infrared is close to 1.0 for almost all surface types, certain surfaces deviate from that behavior over certain spectral bands. With the MIPAS sequence T0728 taken over Arabian peninsula, sand or sandstone desert is assumed to be the dominating surface type. Emissivity of desert type surface deviates strongly from 1.0 between $1000-1300\,\text{cm}^{-1}$, where it drops to about 0.7, and fluctuates between 0.9 and 1.0 for $\nu < 1000\,\text{cm}^{-1}$ (see Fig. 2.7). Thus, influence of emissivity variations is studied with varying $\varepsilon_{\text{surf}}$ between $0.9-1.0$ for microwindows mw1 and mw2 and $0.8-0.95$ for mw3, respectively.

Beside by surface emissivity, the amount of radiation emitted by the surface is determined by its temperature. As default value used in this study, surface temperature is assumed to equal atmospheric temperature at 0 km altitude. Apart from the fact that lower atmospheric profiles

due to cloud interference are not results of the retrieval but a priori values and may therefore deviate from the "real" values, that assumption neglects daytime dependent surface heating and cooling effects. In particular, in desert areas surface temperature can change by ±30 K during 24 hours. With the measurement taken at 10:30 am local time, being close to balanced surface and bottom atmospheric temperature is assumed, i.e. being close to the point, when heating from cool night to hot daytime surface temperature meets atmospheric temperature at 0 km altitude. However, surface temperature effects are examined with T_{surf} varied by ±12 K from the default value of equal atmospheric and surface temperature.

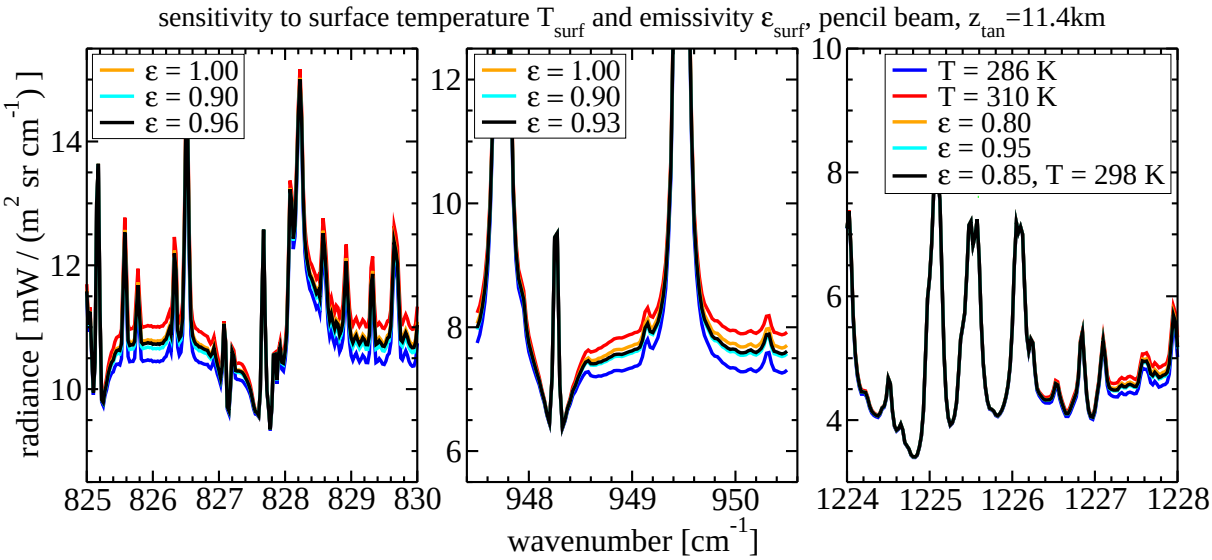

Figure 6.20: *Sensitivity to uncertainties in surface temperature T_{surf} and emissivity $\varepsilon_{\mathrm{surf}}$*

Results of both, varied surface emissivity and temperature are shown in Fig. 6.20. It is found, that a change in surface emissivity is basically negligible at all microwindows, in particular when taking into account instrumental accuracy (see section 6.1). That might be because of no temperature gradient between lowest atmospheric layer and surface. Hence, this finding might not be valid under different conditions. Varying the surface temperature by ±12 K results in rather slight changes in the continuum signal of about ±0.2 (mw3) to ±0.7 mW/(m^2 sr cm^{-1}) (mw1). Due to a opaque atmosphere between surface and LOS, no changes occur around the H_2O and CH_4 lines. In conclusion, compared to effects of most cloud properties on the one hand and tangent altitude uncertainty on the other, spectral variability due to uncertain surface properties is very small and should not effect the derivation of cloud properties significantly.

6.4.9 Conclusions

Effects of cirrus clouds on limb emission spectra have been simulated. The sensitivity of the spectra to macrophysical and microphysical cloud properties (optical depth, cloud top height and geometrical thickness, particle size distribution and crystal habit) has been studied. Furthermore, uncertainties introduced by an insufficient knowledge of surface properties and tangent altitude have been examined.

For thin to subvisible ice clouds, several parameters have been found to primarily result in changes of the broadband continuum signal in atmospheric windows. Cloud optical thickness τ_c is the one of those, that shows a very large variability in nature and, beside that, causes the most significant changes in the continuum signal. Effects of varying cloud top height and cloud geometrical thickness are similar to those resulting from small changes in τ_c. Furthermore, the close relation between effects of only a fractional part of the instrumental field of view observing the cloud and variations in optical thickness of the cloud, as described by Ewen et al. (2005), has been approved.

Using three microwindows in the atmospheric window around 10 μm, it has been shown, that information about size distribution of the ice particles in a cloud as well as about their shape might be derived from simultaneous investigation of different spectral regions. While the aforementioned parameters like cloud optical thickness lead to either enhancement or decrease of the broadband signal in all of the microwindows, these microphysical properties were the only found to cause changes of the continuum intensity in the three windows relative to each other. On the other hand, when examining spectra over a single microwindow of only a few wavenumbers width, effects of particle size and shape are hardly separable from other parameters. Hence, for retrieving microphysical properties it is recommended to use microwindows placed over a wide spectral range for which cloud optical properties vary in different manner depending on particle size.

The large influence of assumptions about cloud position and cloud extent, respectively, in case of thin or subvisible clouds has been demonstrated. First, observing a cloud only in front or behind the tangent point leads to similar spectral behavior as the observation of a whole layer cloud cover of about half optical thickness. That matches the fact, that indeed only about half of the cloud mass as for a whole layer cover is observed by the instrument. Second, a cloud at the observer side of the tangent point leads to a higher response than a cloud at the far side. But, as effects of cloud top height, geometrical thickness and filling of the FOV, cloud position/extent effects can hardly be separated from optical thickness variations.

Inaccuracy in the surface properties has been found to cause only small uncertainties in the simulated spectra compared to effects of the several cloud parameters. Regarding the MIPAS sequence, measured in northern hemisphere summer over desert areas of the Arabian peninsula, the examined range of the surface temperatures might be too small to cover the diurnal temperature cycle. On the other hand, at a local time of observation of 10:30am, surface heating can be assumed to be smaller than 12 K. Concerning inaccuracy of tangent altitude, effects on the spectra have also been observed to be rather small compared to changes by variations of cloud parameters. A large fraction of effects caused by shifted tangent altitude is balanced by an equivalent shift of the cloud's vertical position. The shape of the spectral H_2O features can provide information about tangent altitude, but is highly dependent on the water vapor profile. However, due to the high variability and large uncertainties of the water vapor profile, gaining information from H_2O line shape is very complex. Thus, uncertainties in surface properties or tangent altitude may rather cause biased estimates of cloud optical thickness or result in an offset of cloud height estimate, respectively.

6.5 Retrieval Results

Cirrus clouds have been observed by MIPAS on July, 17th, 2003 over the Arabian peninsula (sequence T0728) at tangent altitude of 15 km and below. For deriving properties of these clouds, measurements of sweep 13 ($z_{\mathrm{tan}} \approx 15\,\mathrm{km}$) and sweep 14 ($z_{\mathrm{tan}} \approx 12\,\mathrm{km}$) are used. It is assumed, that both sweeps observe the same, homogeneous cloud, i.e. that average cloud properties do not vary significantly within both observed fractions of the cloud.

The derivation of cirrus properties is based on the sensitivity study, discussed in the previous section. Apart from variation of single parameters of the cloud in the sensitivity study, simulations with combinations of cloud properties changed have been carried out in order to obtain a best fit of the spectra in the 3 microwindows for sweeps 13 and 14 simultaneously. Out of the cloud properties examined in the sensitivity study, ice water path, cloud optical and geometrical thickness, cloud top height, position and particle size are estimated. No information about crystal habit has been derived, but the cloud has been assumed to consist of solid columns. Atmospheric conditions as well as surface properties and tangent altitudes have been used as described in section 6.3 and taken to be "true".

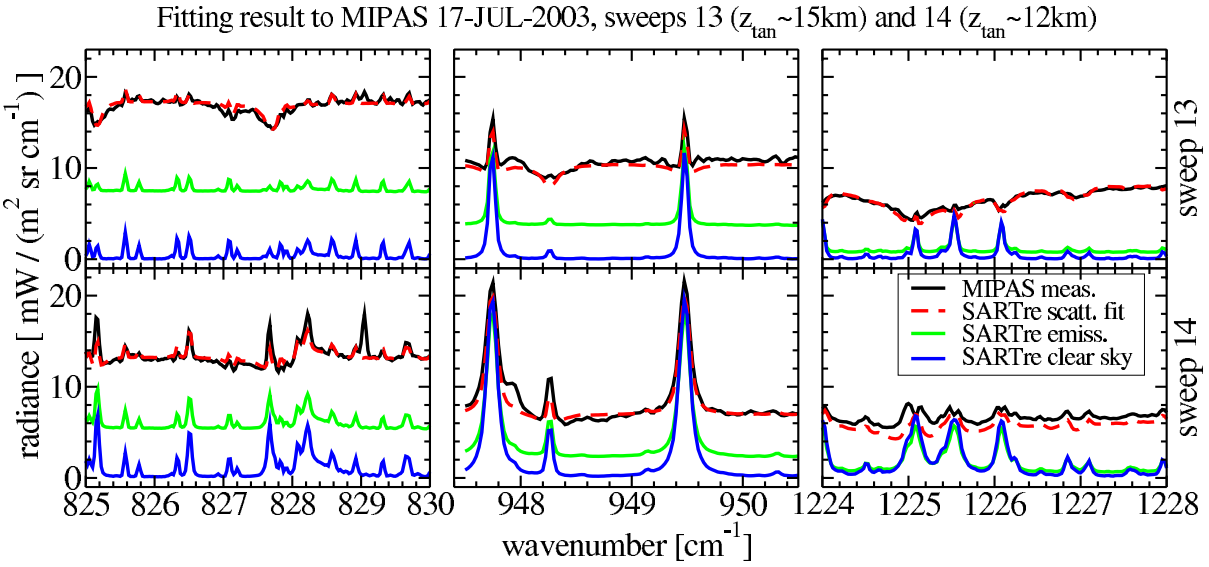

Figure 6.21: *Measured MIPAS spectra and best-fit SARTre modeled spectra of sweep 13 (upper panel) and sweep 14 (lower panel). For comparison simulated spectra for clear-sky conditions and for cloudy conditions with scattering contribution neglected are added.*

To measure the quality of the fits, the quantity

$$\chi^2 = \sum_{i=1}^{N_\nu} \frac{|I_{\mathrm{meas}}(\nu_i) - I_{\mathrm{sim}}(\nu_i)|^2}{\epsilon_{\mathrm{meas}}(\nu_i)^2} \tag{6.5}$$

is used (Ewen et al., 2005), where $I_{\mathrm{meas}}(\nu_i)$ and $I_{\mathrm{sim}}(\nu_i)$ denote the MIPAS measured and the SARTre modeled intensity at spectral point ν_i, respectively. $\epsilon_{\mathrm{meas}}(\nu_i)$ is the uncertainty in $I_{\mathrm{meas}}(\nu_i)$ induced by measurement errors, described by NESR of $0.5\,\mathrm{mW/(m^2\,sr\,cm^{-1})}$ for microwindows mw1 and mw2 in MIPAS channel A and $0.2\,\mathrm{mW/(m^2\,sr\,cm^{-1})}$ for mw3 in MIPAS

channel B. Using the normalized quantity $\chi^2_{\text{norm}} = \chi^2/N_\nu$, a good fit is defined by $\chi^2_{\text{norm}} \approx 1$. The best-fit solution is found, when the spectra minimise χ^2_{norm} over the 3 microwindows for the two subsequent sweeps.

Best fitting simulations from the set of calculated spectra are found for a cloud with

- ice water path IWP $= 0.1\,\text{g/m}^2$
- optical thickness $\tau_\text{c} = 0.008$
- size distribution "liou_full" with effective particle size $D_\text{e} = 10.5\,\mu\text{m}$
- top height $z_\text{top} = 15.5\,\text{km}$
- geometrical thickness $\Delta z = 1.0\,\text{km}$
- cloud only located on the observer side of the sweep 14 LOS with the tangent point located below the cloud, but on both sides for sweep 13, where the tangent point is located inside the cloud..

Corresponding simulated spectra together with the MIPAS measurements are presented in Fig. 6.21. Intensity deviations as well as percentage differences between the best-fit spectra and measurement are shown in Fig. 6.22.

6.5.1 Discussion

For all three microwindows of sweep 13 as well as mw1 and mw2 of sweep 14, the spectra match the measurement well, particularly concerning the broadband continuum signal. The continuum signal in mw3 of sweep 14 is significantly underestimated, but the spectral features are found to be similar to the measured ones outside the H_2O and CH_4 dominated region. According to the sensitivity study results, this might be due to the particle size guess being inappropriate for the cloud sample observed by sweep 14.

Furthermore, it has been possible to roughly reproduce the water vapor signatures observed in the measured MIPAS spectra Larger deviations are found again in microwindow mw3 of sweep 14. There, none of the spectra in the simulated set meets the spectral behavior of the H_2O line at $1225.1\,\text{cm}^{-1}$. It is highly likely, that this mismatch is caused by the water vapor mixing ratio, used for the modeling, being far off the true profile in the troposphere. As no retrieval has been done from cloud interfered measurements, the profile below 18 km resembles the a priori profile. On the other hand, it is well known, that water vapor content has a high variability in the Earth's atmosphere in time and space. In particular, it may be questionable, whether a midlatitude climatology profile matches the atmospheric conditions over a desert area. Furthermore, it had been observed, e.g. by Del Genio et al. (2002), that cirrus often forms in layers of enhanced relative humidity. Using an a priori profile, this moist layer is surely missed.

In general deviations are larger in and around strong trace gas lines than in the continuum. Since not included in the simulation, modeled intensities differ strongly from the measurement around the OCS line in microwindow mw1 and the SF_6 line in mw2. Nevertheless, results for sweep 13 are to a great extent found within measurement accuracy of the instrument. Deviations around single lines are observed to be more pronounced in sweep 14, which may result from the higher uncertainties in the mixing ratio and temperature profiles of the troposphere in and below the cloud. Also, neglecting further atmospheric constituents dominant in the troposphere,

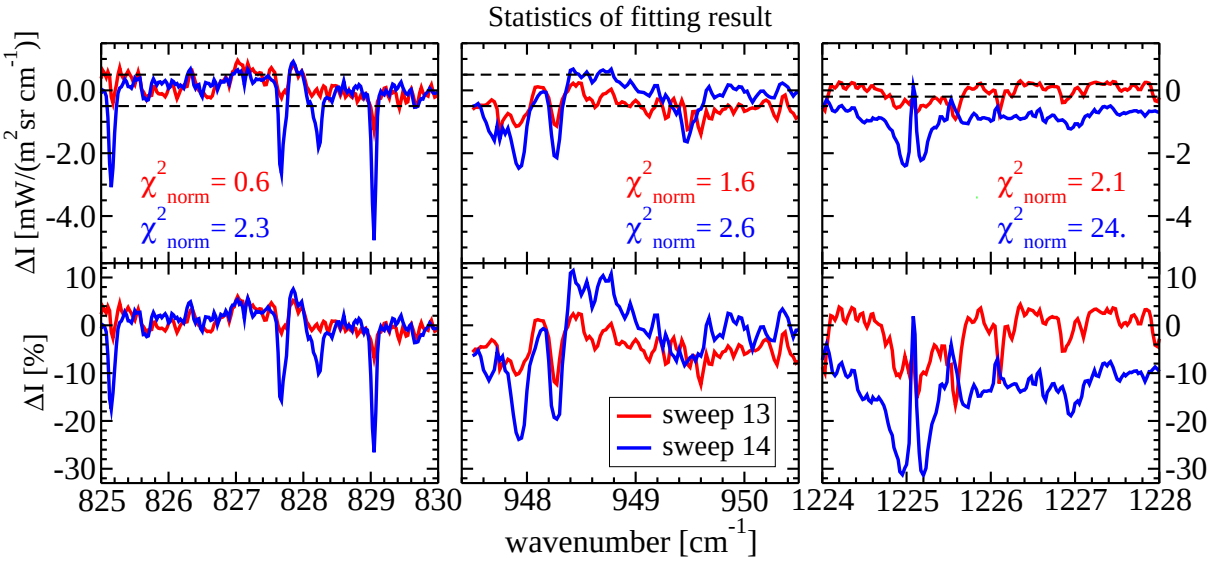

Figure 6.22: *Deviations of intensities (upper panel) and percentage differences (lower panel) of modeled and measured spectra. Black lines in the upper panel denote channel specific NESR of MIPAS.*

e.g. boundary layer aerosols, which modify radiation originating from the surface and the lower troposphere as well, might contribute.

However, the properties derived for the observed cirrus cloud seem plausible. With a top height of about 15.5 km, the cloud is located right below the tropopause. At ambient temperature of around −70 °C small particles of pristine crystal shape are expected to dominate, matching the finding of effective particle size of about 10 μm. Although the observed cirrus with an IWP of 0.1 g/m^2, which is subvisible in the mid-IR, has a higher optical thickness of $\tau_c^{vis} \approx 0.02$ in the visible, it can be hardly detected by nadir and slant looking instruments. For example, from MODIS data taken about an hour later no cirrus was detect. The MERIS cloud mask (Preusker et al., 2005) has detected some "clouds" below the southern part of the MIPAS line of sight. Although these might not necessarily be clouds, but could also be some artefacts e.g. from surface effects [2], the RGB-composite indicates some clouds in the southernmost part of the scene as well. Taking into account that those clouds originate from above the sea, they might well be convective clouds producing thin anvil cirrus. That furthermore means, part of the clouds detected by MERIS could even be some thicker part of the anvil cirrus. That basically matches the finding from the MIPAS retrieval, that the cloud at the lower tangent altitude measurement is located on the observer side of the LOS. Besides, the development of the anvil cirrus originating from southern part and moving towards north, might also indicate a change in particle size. Dominance of freshly forming, and thus very small particle in the southernmost part vs. further developed crystals towards north might explain the deviations in the fitted spectra.

[2] Compare the region of the mouth of Euphrat and Tigris in Fig. 6.1. From the RGB-composite it becomes obvious that the "clouds" detected there are rather effects of water containing a large amount of suspended matter that causes high backscattering.

To emphasize the effects of cirrus clouds in limb emission spectra, model results for clear-sky conditions and for cloudy conditions with scattering into the LOS neglected have been plotted for comparison in Fig. 6.21. For the cloud with above mentioned properties derived, 40 – 90 % of radiation measured outside the very strong lines result from scattering into the line of sight.

6.5.2 Conclusions

By modeling limb emission measurements with SARTre, it was possible to reproduce the major characteristics of cirrus cloud interfered spectra as observed by MIPAS. Based on a sensitivity study, cloud micro- and macrophysical properties were estimated by fitting simulated spectra to MIPAS measurements simultaneously in three distinct microwindows between 825 – 1230 cm^{-1} and two subsequent tangent altitudes. Best-fitting spectra match the measurement well concerning both, the broadband continuum signal and distinct H_2O absorption features due to scattering of radiation into the LOS. Remaining deviations between simulation results and MIPAS measurements have been discussed as well as the plausibility of the estimated cloud properties. In summary, the SARTre model has been proved to be an appropriate tool for studying scattering effects in thermal emission spectra.